Journal for ImmunoTherapy of Cancer

Adaptive single-KIR$^+$NKG2C$^+$ NK cells expanded from select superdonors show potent missing-self reactivity and efficiently control HLA-mismatched acute myeloid leukemia

Alvaro Haroun-Izquierdo ,[1] Marianna Vincenti ,[2] Herman Netskar ,[2] Hanna van Ooijen,[3] Bin Zhang,[4] Laura Bendzick,[4] Minoru Kanaya ,[2] Pouria Momayyezi,[1] Shuo Li,[2] Merete Thune Wiiger,[2] Hanna Julie Hoel,[2] Silje Zandstra Krokeide,[2] Veronika Kremer,[1] Geir Tjonnfjord,[5] Stéphanie Berggren,[6] Kristina Wikström,[6] Pontus Blomberg,[6] Evren Alici,[7] Martin Felices ,[4] Björn Önfelt,[3,8] Petter Höglund,[7,9] Bahram Valamehr,[10] Hans-Gustaf Ljunggren,[1] Andreas Björklund,[1,11] Quirin Hammer,[1] Lise Kveberg ,[2] Frank Cichocki,[4] Jeffrey S Miller,[4] Karl-Johan Malmberg ,[1,2] Ebba Sohlberg [1]

To cite: Haroun-Izquierdo A, Vincenti M, Netskar H, *et al*. Adaptive single-KIR$^+$NKG2C$^+$ NK cells expanded from select superdonors show potent missing-self reactivity and efficiently control HLA-mismatched acute myeloid leukemia. *Journal for ImmunoTherapy of Cancer* 2022;**10**:e005577. doi:10.1136/jitc-2022-005577

► Additional supplemental material is published online only. To view, please visit the journal online (http://dx.doi.org/10.1136/jitc-2022-005577).

K-JM and ES are joint last authors.

Accepted 24 September 2022

For numbered affiliations see end of article.

Correspondence to
Professor Karl-Johan Malmberg; k.j.malmberg@medisin.uio.no

ABSTRACT

Background Natural killer (NK) cells hold great promise as a source for allogeneic cell therapy against hematological malignancies, including acute myeloid leukemia (AML). Current treatments are hampered by variability in NK cell subset responses, a limitation which could be circumvented by specific expansion of highly potent single killer immunoglobulin-like receptor (KIR)$^+$NKG2C$^+$ adaptive NK cells to maximize missing-self reactivity.

Methods We developed a GMP-compliant protocol to expand adaptive NK cells from cryopreserved cells derived from select third-party superdonors, that is, donors harboring large adaptive NK cell subsets with desired KIR specificities at baseline. We studied the adaptive state of the cell product (ADAPT-NK) by flow cytometry and mass cytometry as well as cellular indexing of transcriptomes and epitopes by sequencing (CITE-Seq). We investigated the functional responses of ADAPT-NK cells against a wide range of tumor target cell lines and primary AML samples using flow cytometry and IncuCyte as well as in a mouse model of AML.

Results ADAPT-NK cells were >90% pure with a homogeneous expression of a single self-HLA specific KIR and expanded a median of 470-fold. The ADAPT-NK cells largely retained their adaptive transcriptional signature with activation of effector programs without signs of exhaustion. ADAPT-NK cells showed high degranulation capacity and efficient killing of HLA-C/KIR mismatched tumor cell lines as well as primary leukemic blasts from AML patients. Finally, the expanded adaptive NK cells had preserved robust antibody-dependent cellular cytotoxicity potential and combination of ADAPT-NK cells with an anti-CD16/IL-15/anti-CD33 tri-specific engager led to near-complete killing of resistant CD45^{dim} blast subtypes.

Conclusions These preclinical data demonstrate the feasibility of off-the-shelf therapy with a non-engineered, yet highly specific, NK cell population with full missing-self recognition capability.

WHAT IS ALREADY KNOWN ON THIS TOPIC

⇒ Adoptive natural killer (NK) cell therapy in combination with hematopoietic stem cell transplantation can provide cure for acute myeloid leukemia (AML) but is in part dependent on variable NK cell reactivity. Adaptive NK cells are a highly potent NK cell subset that can be used to maximize 'missing-self' reactivity against tumor cells.

WHAT THIS STUDY ADDS

⇒ It describes a novel GMP-compliant protocol to expand clinically relevant numbers of single self-killer immunoglobulin-like receptor$^+$ adaptive NK cells from third-party 'superdonors' that provide strong alloreactivity in a mouse model of AML as well as against primary AML blasts ex vivo.

HOW THIS STUDY MIGHT AFFECT RESEARCH, PRACTICE OR POLICY

⇒ These preclinical data demonstrate the feasibility of cell therapy with a non-engineered and yet highly specific NK cell population with maximized missing-self recognition.

INTRODUCTION

Natural killer (NK) cells can mediate strong antitumor immunity, which is being explored in immunotherapy strategies for human malignancies. Adoptive transfer of allogeneic

NK cells has a good safety profile without cytokine release syndrome, neurotoxicity, or GvH disease and has shown efficacy for subgroups of refractory leukemia patients.[1–5] Current approaches to generate NK cells for therapy include sourcing and expanding NK cell lines, donor-blood and cord-blood NK cells, and inducible pluripotent stem cell (iPSC)-derived NK cells using feeder cell lines and cytokines.[6] Despite promising results, the persistence, and variable antitumor responses of different NK cell subsets along with high diversity of NK cell repertoires in healthy donors,[7] represents a potential limitation of donor-derived NK cell-based therapy strategies. Identifying biology-driven approaches that can enhance these attributes prior to adoptive transfer and establishing selection procedures for optimal donors therefore represent key bottlenecks in the field.

Early observations showed that NK cell cytotoxicity was triggered by tumor cells that lacked expression of some or all self-MHC class I molecules, referred to as 'missing-self' recognition.[8] Therefore, it was postulated that NK cells might be particularly effective when transferred across HLA barriers,[9 10] where NK cell alloreactivity would be unleashed through mismatch between donor NK clones bearing inhibitory killer immunoglobulin-like receptor (KIR) specific for self-HLA class I molecules ('self-KIR') and recipient cells lacking the cognate HLA class I ligands. For such an NK cell-mediated graft-versus leukemia (GvL) effect to take place, there must be a mismatch in any of the three major KIR-KIR ligand (KIR-L) settings (KIR2DL1 missing HLA-C2, KIR2DL3 missing HLA-C1, or KIR3DL1 missing HLA-Bw4). The importance of NK cell alloreactivity was elegantly explored in landmark studies by the Velardi group, where the size of the alloreactive NK subset was linked to improved outcomes in patients, both in hematopoietic stem cell transplantation (HSCT) and later in adoptive NK cell transfer in acute myeloid leukemia (AML).[2 10 11] Studies investigating a KIR-L mismatch effect have not always been conclusive though, which may in part be related to the variable frequency of the alloreactive NK cell subset,[12] in turn due to the stochastic expression of KIR.[13] Therefore, selectively expanding the alloreactive subset prior to adoptive NK cell transfer to increase missing-self reactivity[14] would be greatly desired and could lead to clinical benefits.

NK cell differentiation spans from naive $CD56^{bright}$ cells to highly differentiated $CD56^{dim}$ adaptive NK cells induced by cytomegalovirus (CMV) infection.[15 16] Adaptive NK cells are characterized by the expression of the activating receptor CD94/NKG2C (NKG2C), whose cognate ligand HLA-E also binds to the inhibitory receptor CD94/NKG2A (NKG2A). Engagement of NKG2C by peptide-stabilized HLA-E can elicit effector functions and support adaptive NK cell expansion in vitro.[17–20] Apart from NKG2C, the adaptive NK cell signature is characterized by a unique surface phenotype, distinct patterns of transcription factors and signaling molecules as well as altered DNA methylation patterns.[21–23] Adaptive NK cells have a high effector molecule content and an increased capacity for IFN-γ production and antibody-dependent cellular cytotoxicity (ADCC).[18 21 24 25] Intriguingly, their unique and preferential expression of a single self-KIR[18] make them especially attractive for strategies aiming at exploiting missing-self recognition since they will demonstrate predictable alloreactivity in HLA-mismatched settings. In allogeneic HSCT, reactivation of CMV and concurrent expansion of adaptive NK cells has been associated with remarkable reductions in AML relapse rates,[26–29] highlighting their clinical relevance and potential.

We have previously developed an HLA-E feeder-based platform for selective expansion of adaptive NK cells, leading to highly pure populations with potent alloreactivity against primary acute lymphoid leukemia.[30] Here, we used CD3/CD19-depleted cryopreserved cell material from 'superdonors' that harbored large $NKG2C^+$ adaptive NK cell subsets with single self-KIR expression, to generate high expansion rates of adaptive NK cells. ADAPT-NK cells largely maintained their adaptive signature, and demonstrated strong alloreactivity against tumor cell lines, in an in vivo AML model and against primary AML samples. Finally, we show that a combination of ADAPT-NK cells with an immune engager enhances reactivity against more resistant AML blast subtypes, broadening the therapeutic utility of the ADAPT-NK cell platform.

METHODS

Additional Methods can be found in online supplemental materials.

Human participants and cell processing

Healthy CMV-seropositive blood donors with large pre-existing adaptive NK cell subpopulations (>20% of $NKG2C^+$ with single self-KIR2DL1 or KIR2DL3 expression, denoted as 'superdonors') were included in the study. Peripheral blood monunuclear cells (PBMCs) were isolated from buffy coats using Lymphoprep and CD3/CD19-depleted as per manufacturer's instructions (Miltenyi Biotec). PBMC were also obtained from leukapheresis products that were subsequently CD3/CD19-depleted by CliniMacs (Miltenyi). Depleted cell products were cryopreserved in 90% heat-inactivated fetal bovine serum (FBS,Sigma-Aldrich) or 90% autologous plasma with 10% DMSO until use. To determine donor HLA-C type, DNA was isolated using a commercial kit (DNeasy Blood & Tissue, Qiagen) and the KIR HLA ligand kit was used (Olerup SSP). CMV serology was determined using an ELISA-based assay on plasma obtained during sample preparation. Purified nuclear CMV antigen (AD 169) was used, and the cut-off level for seropositivity was an absorbance of ≥0.2 at a dilution of 1/100.

ADAPT-NK cell expansion protocol

CD3/CD19-depleted PBMC were co-cultured with 100 or 200 Gy irradiated K562 feeder cells transfected with lentiviral construct to express high levels of HLA-E with an HLA-G-leader-derived peptide (Fate Therapeutics, details

in 'Genetic cell engineering') at a 1:2 ratio in G-Rex24 plates (Wilson Wolf) at 0.5×10^6 total cells/cm^2. Cells were cultured in GMP-grade Stem Cell Growth Medium (CellGenix) supplemented with 10% human ab serum (TCS Biosciences or Access Biologicals), 2mM L-glutamine (Cytiva -FisherScientific) and 100 IU/mL human recombinant IL-2 (Proleukin) for 11 days with 60% medium exchange on day 7, and IL-2 addition days 4, 7 and 10.

Flow cytometry and mass cytometry

NK cell phenotype and function was evaluated using standard protocols for flow- and mass cytometry. Samples were acquired on a BD LSRII, or LSR-Fortessa 18-color flow cytometer (BD Biosciences) or on a Helios CyTOF instrument (Fluidigm), and data were analyzed with FlowJo software V.10 (BD Biosciences) and R (R Core Team, 2019). Details are available in online supplemental materials including flow cytometry antibodies (online supplemental sTable 1) and mass cytometry antibodies (online supplemental sTable 2).

Cellular indexing of transcriptomes and epitopes by sequencing CITE-Seq

CITE-seq was performed as outlined in Biolegend 'TotalSeqTM-A Antibodies and Cell Hashing with 10X Single Cell 3' Reagent Kit V.3 3.1 Protocol' with minor modifications. Briefly, cells were stained with CD56-biotin (REA 196), followed by TotalSeq antibodies and TotalSeq streptavidin-PE and Live/Dead Aqua (Invitrogen) and subsequently sorted for viable $CD56^+$ cells by flow cytometry (online supplemental sFigure 2A,B). To distinguish day 0 and day 11 cells, streptavidin-PE conjugated to different oligos were used, and equal number of sorted viable $CD56^+$ cells from the two cell preparations were pooled as one sample. This was followed by standard 10X Genomics library preparation and sequencing workflow (Genomics Core Facility OUH/UiO, Oslo, Norway). Sequencing was performed with the recommended read lengths on the NextSeq500 sequencer (Illumina) and detailed description of the analysis of CITE-seq data is available in online supplemental materials. For network analyses, the DifferentialNet database[31] (integrated data from experimentally detected protein–protein interactions (PPIs), and RNA sequencing gathered by the Genotype-Tissue Expression consortium) was used to generate tissue-specific (whole blood) PPI networks that were visualized with NetworkAnalyst V.3.0. Enrichment analyses were performed in NWA3.0 with the Gene Ontology (Biological Processes) database.

Tumor cell lines

The K562 cell line (chronic myeloid leukemia) and 721.221 (EBV-transformed B cell line) were obtained from ATCC (American Type Culture Collection). HL-60 (AML) was obtained from the Miller lab. PANC-1 (Pancreatic ductal adenocarcinoma) and A549 (lung adenocarcinoma) were obtained from Fate Therapeutics. K562, A549 and PANC-1 along with NALM-6 (B cell acute lymphoblastic leukemia) and BJAB (Burkitt-like Lymphoma) were reauthenticated using STR fingerprinting (ATCC) .

AML patient samples

EDTA blood samples were collected at diagnosis from AML patients (Dep. of Hematology, Oslo University Hospital, Oslo, Norway). PBMC were isolated by Lymphoprep and cryopreserved in RPMI 1640 with 60% FBS and 10% DMSO. Patients were genotyped by Illumina NGS platform (Dep. of Immunology, Oslo University Hospital, Oslo, Norway) and for this study, samples were selected from patients of either HLA-C1/C1 or HLA-C2/C2 haplotypes.

Flow cytometry-based NK cell functional assays

NK cell degranulation and cytokine production was evaluated by mixing ADAPT-NK products at different effector to target (E:T) ratios with tumor targets in 6 hour co-cultures. To measure ADCC, anti-CD20 (MabThera, 1 µg/mL) was added to co-cultures with 721.221 cells. Phorbol-12-myristate-13-acetate (50 ng/mL) + ionomycin (1 µg/mL) (Sigma) was used as positive control. In cytotoxicity assays, target cells were pre-stained with CellTrace Violet (Invitrogen), and FITC-DEVD-FMK (Abcam) to detect active Caspase-3, was added at the start of the incubation. Dead/dying cells were defined as $CellTrace^+$ $Caspase\text{-}3^+$ and/or dead cell $marker^+$ and specific cytotoxicity was calculated as: $(\%\ dead^{\ experimental} - \%\ dead^{\ target\ only}) \div (100\% - \%\ dead^{\ target\ only}) \times 100\%$. For competitive cytotoxicity assays, K562 expressing an HLA-C1-or HLA-C2-dimer were stained with two different concentrations of CellTrace Violet prior to being mixed at a 1:1 ratio and subsequently seeded at different E:T ratios with ADAPT-NK cells. Cytokine stimulations with IL-12 (10 ng/mL) and IL-18 (10 ng/mL) (both Biotechne) were performed for 25 hours. Further experimental details are provided in online supplemental methods.

Genetic cell engineering

Engineered cell lines used in this study are described in detail in online supplemental material. Briefly, for the expansion of ADAPT-NK cells, K562 cells (ATCC Cat: CCL-243) were engineered by Fate Therapeutics using a third-generation lentiviral transfer plasmid designed to contain a chimeric protein with the HLA-G leader peptide (1-24) and the mature *HLA-E*0103* (22-358) driven by an EF1α promoter. For additional HLA-C and HLA-E variants, K562 were engineered in-house using VSV-G-pseudotyped lentiviral particles with a mammalian LeGO-G2 expression vector, to express the following synthetic proteins: β2m–HLA-C1 (*HLA-C*07:01*) single chain dimer (HLA-C1-dimer); β2m–HLA-C2 (*HLA-C*04:01*) single chain dimer (HLA-C2-dimer) and $HLA\text{-}G_{3\text{-}11}$–β2m–*HLA-E*01:01* single chain trimer (HLA-E-trimer). For HLA-E knock-out in NALM-6 cells, Cas9 and a pool of synthetic guide RNAs (sgRNA) (CRISPRevolution sgRNA EZ Kit, Synthego) were used. Single cells were sorted on a FACS Aria II (BD Biosciences) to establish

multiple clones. DNA sequencing and flow cytometry confirmed HLA-E depletion in the selected clones used in the study. HLA-E sgRNAs further targeted the HLA-C locus resulting in a combined KO for NALM-6.

Serial killing assays

The cytotoxic potential of individual NK cells was evaluated using a previously described microwell chip screening assay.[32] Briefly, labeled NK cells and labeled target cells were seeded in a microwell chip containing complete RPMI supplemented with Sytox Green (Thermo Fisher). Cells stochastically distributed in the 8064 60-µm-wide wells at an average E:T ratio of 1:5. The co-cultures were imaged every 3 hours for 15 hours using a LSM 880 (Carl Zeiss AG) inverted confocal microscope. The images were processed using a custom-built MATLAB script whereby live and dead cells were quantified at all time points, and for each condition a minimum of 500 wells containing a single NK cell at start along with at least 4 live target cells, were included for analysis. Further details are available in online supplemental material.

IncuCyte measurement of tumor killing

Tumor killing was measured in real-time using the IncuCyte S3 platform. Detailed description of the protocol is available in online supplemental material. Briefly, target cells stably expressing NucLight Red (Essen Biosciences) were overnight rested and subsequently co-cultured with ADAPT-NK cells at different E:T ratios. Images (3/well) from at least two technical replicates for each condition were acquired every 90 min for 48 hours, using a ×10 objective lens and analyzed by IncuCyte Controller v2020A (Essen Biosciences). Graphed readouts represent percentage live target cells.

In vivo AML tumor model

Detailed description of the protocol is available in online supplemental material. Briefly, NOD.Cg-PrkdcscidIl2rgtm1Wjl/SzJ mice (NSG, Jackson Laboratories) mice were injected intravenously with HL-60 cells stably expressing firefly luciferase (1.5×10^6/mouse). Four control mice on the same background received no injections. After allowing tumors to engraft for 4 days, bioluminescence imaging was performed, and mice were randomized into three groups: tumor alone, HLA-C/KIR matched ADAPT-NK cells (flat-dose 5×10^6/mouse) or HLA-C/KIR mismatched ADAPT-NK cells (flat-dose 5×10^6/mouse). Mice receiving NK cell injections were also injected intraperitoneally with IL-15 (National Cancer Institute, 6 ug/mouse) twice weekly for 3 weeks. Bioluminescence imaging was performed weekly to track tumor burden using the IVIS Spectrum In Vivo Imaging System (Perkin-Elmer).

Statistical analyses

Statistical analyses and visualization were performed using Prism V.9 (GraphPad) and R with the *ggplot2* and *dunn.test* packages. Paired Student's t-tests were used for paired comparisons. Repeated measures one-way analysis of variance (ANOVA) with Tukey's correction was used to analyze three groups (flow, mass- cytometry and CITE-Seq). One-way ANOVA with Šidák's multiple comparison correction was performed for NK cytotoxicity assays evaluated by flow cytometry and in the IncuCyte platform. Two-way ANOVA with Tukey's multiple comparison correction was performed to analyze the in vivo AML tumor model. Nonparametric Spearman-rank correlation was performed for evaluation of HLA-E in AML patient samples and NK cell cytotoxicity against these.

RESULTS

Efficient expansion of single-self-KIR$^+$NKG2C$^+$ adaptive NK cells (ADAPT-NK)

NKG2C$^+$ adaptive NK cells tend to express only a single self-KIR, a fact that translates to high alloreactive potential if transferred to recipients with KIR-L (HLA-C) mismatch.[18 30] Re-examining data from our previously published cohort of healthy blood donors,[18] 48/202 donors had a large (over 20%) NKG2C$^+$ adaptive NK cell subset, and of those, 26 had a clear single-self KIR2DL1$^+$KIR2DL3$^-$ or KIR2DL1$^-$KIR2DL3$^+$ expression profile (figure 1A,B) and were subsequently denoted as 'superdonors'. Based on CD3/CD19-depleted material from these select superdonors, a GMP-compliant protocol to expand adaptive NK cells was developed (figure 1C). Monocytes and feeder cells were undetectable in the co-cultures by day 7, concomitant with a rise in NK cell numbers (figure 1D,E). On day 11, a median of 91% of NK cells were NKG2C$^+$ and 81% had single-self-KIR expression (either KIR2DL1$^+$KIR2DL3$^-$ or KIR2DL1$^-$KIR2DL3$^+$, figure 1F,G). Hereafter, we refer to this expanded adaptive NK cell product as 'ADAPT-NK' cells. While CD57 expression declined slightly, less than 20% of cells expressed NKG2A post-expansion (figure 1F,G). Replicate expansions of cell material obtained from the same donor and from several donations, gave stable results (median 88% NKG2C$^+$, SD 3.64% figure 1H). We achieved a median of 470-fold expansion of adaptive NK cells with some donors displaying over 1000-fold expansion rates (figure 1I). Thus, the developed expansion protocol produced high fold changes of single self-KIR$^+$NKG2C$^+$ adaptive NK cells in 11 days, opening an avenue for clinical development.

ADAPT-NK cells retain an adaptive transcriptional signature with activation of effector programs and without signs of exhaustion

To assess the adaptive state in NKG2C$^+$ NK cells pre-expansion and post-expansion, we performed extended phenotyping by flow cytometr and mass cytometry (figure 2 and online supplemental sFigure 1) as well as cellular indexing of transcriptomes and epitopes by sequencing (CITE-Seq) (figure 2 and online supplemental sFigure 2). For mass cytometry, gating was performed on viable CD56$^+$ NK cells and visualized in t-SNE plots, with distinct topological regions corresponding to day 0 and day 11 NK cells (figure 2A and online supplemental sFigure

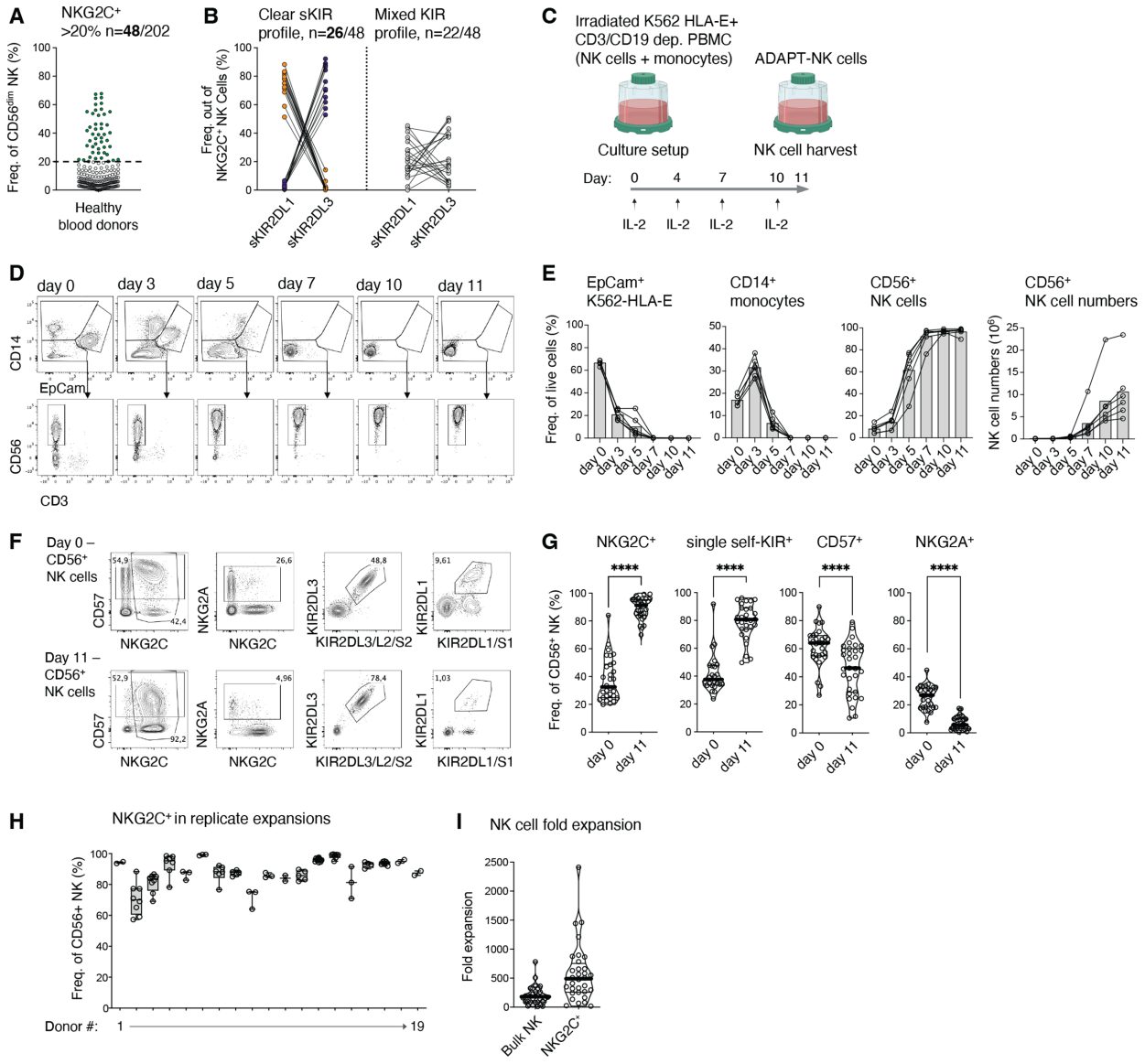

Figure 1 Selective expansion of single-self KIR$^+$NKG2C$^+$ adaptive NK cells. (A) NKG2C$^+$ out of CD56^{dim} NK cells in a cohort of 202 healthy blood donors and in (B) KIR2DL1$^+$KIR2DL3$^-$ or KIR2DL1$^-$KIR2DL3$^+$ out of NKG2C$^+$CD56^{dim} NK cells in the 48 healthy blood donors with over >20% NKG2C$^+$ NK cell subsets. (C) ADAPT-NK protocol design. Flow cytometry analysis of (D, E) EpCam$^+$ K562-HLA-E feeders, CD14$^+$ monocytes and CD56$^+$ NK cells on days 0–11 and (F, G) NKG2C$^+$, KIR2DL1$^+$ KIR2DL3$^-$ or KIR2DL1$^-$ KIR2DL3$^+$ ('single self-KIR'), CD57$^+$ and NKG2A$^+$ among total CD56$^+$ NK cells on day 0 and day 11. (H) NKG2C$^+$ frequencies on day 11 where each dot represents a separate expansion of the same donor material. (I) Fold expansion in cell numbers of total and NKG2C$^+$ ADAPT-NK cells on day 11. (A), n=202, (B), n= 48,) (E), n=6, (G-I), n=27–31, in G and I the median of each donor from 34 independent experiments is shown. (H) n=19 from 2–10 independent experiments. Statistical differences were tested using paired t-tests, *p<0.05, **p<0.01, ***p<0.001, ****p<0.0001. KIR, killer immunoglobulin-like receptor; NK, natural killer; PBMC, peripheral blood monunuclar cells.

1A). On day 0, NKG2C$^+$ cells displayed low expression of NKp30, Siglec-7, PLZF, CD38 and high expression of CD2 as compared with NKG2C$^-$ conventional NK (cNK) cells in accordance with previously published phenotypes.[22 33] In addition to NKG2C and single-KIR on ADAPT-NK cells, key adaptive markers such as CD16, CD2 and Siglec-7 were similarly expressed post-expansion whereas CD38, NKp30, PLZF and FcεRIγ were upregulated as compared with resting NKG2C$^+$ adaptive NK cells (figure 2A,B, significance given in online supplemental sFigure 1C). Further, activation-related TIM-3, HLA-DR, CD25, CD69 and CD98 and inhibitory check point molecules TIGIT, TACTILE, PD-1 and LAG-3 were upregulated. Concomitantly, perforin and DNAM-1 were maintained at a high expression level and granzyme B and NKG2D levels were upregulated (figure 2A,B and online supplemental sFigure 1D).

The transcriptional profile of pre-expansion and post-expansion NK cells was interrogated using CITE-Seq (8013 cells sequenced, online supplemental sFigure 2A,B), revealing distinct clusters corresponding to day 0 *KLRC2* cNK and *KLRC2*$^+$ adaptive NK cells as well as

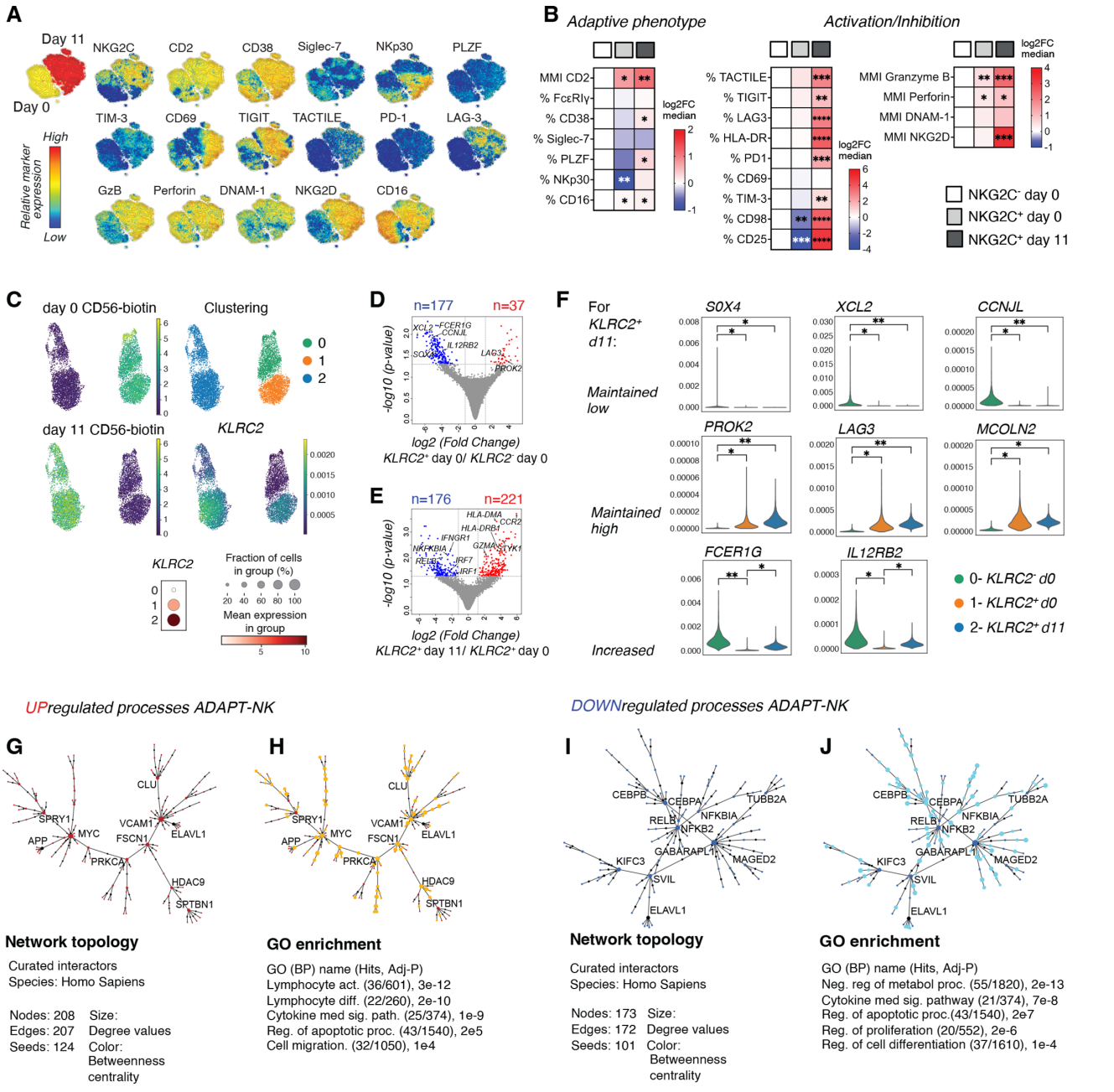

Figure 2 ADAPT-NK cells show a retained adaptive transcriptional signature with activation of effector programs. Extended phenotyping by flow cytometry and mass cytometry as well as CITE-Seq analysis. (A) Relative expression for assessed markers by mass cytometry shown on a t-SNE clustering of sampled events from all individuals (day 0 n=4, day 11 n=6). (B) Frequencies of marker expression or mean metal intensity depicted as median log2 fold change as compared with NKG2C⁻ day 0 from flow- and mass cytometry data. Significances in heatmaps are given as compared with NKG2C⁻ day 0. (C) UMAP embedding of the CITE-seq data colored based on CD56-biotin labeling for day 0 and day 11, cluster assignment (0–2) and expression of KLRC2 in those clusters. Dotplot showing expression of KLRC2 by cluster. (D) 177 downregulated (blue) and 37 upregulated (red) DE genes between KLRC2⁺ day 0 and KLRC2⁻ day 0 and (E) 176 downregulated (blue) and 221 upregulated (red) DE genes between KLRC2⁺ day 0 and KLRC2⁺ day 11 after filtering for log2FC>1.2. (F) Relative gene expression of selected adaptive genes. 'Maintained' indicates significance of *KLRC2*⁺ day 11 to *KLRC2*⁻ day 0 while non-significant to *KLRC2*⁺ day 0. (G) Topology and content of the protein-protein interaction (PPI) network driven by upregulated DE genes for day 11 *KLRC2*⁺ as compared with day 0 *KLRC2*⁺ NK cells. (H) Gene set enrichment analysis of the Steiner forest PPI network with genes that when identified in GO (BP) processes were highlighted (orange). (I) Topology and content of the PPI Steiner forest network driven by downregulated DE genes for day 11 *KLRC2*⁺ as compared with day 0 *KLRC2*⁺ NK cells. (J) GSEA of the PPI network with genes that when identified in GO (BP) processes were highlighted (teal). For flow cytometry and mass cytometry n=4–7, CITE-seq n=1. *p<0.05, **p<0.01, ***p<0.001, ****p<0.0001, in one-way analysis of variance (ANOVA) with Tukey's correction. BP, biological process; GSEA, gene set enrichment analysis; DE; differentially expressed; GO; gene ontology; GSEA, gene set enrichment analysis; PPI, protein–protein interaction; t-SNE, t-distributed stochastic neighbor embedding; UMAP, uniform manifold approximation and projection.

day 11 *KLRC2*$^+$ NK cells (figure 2C). At baseline, *KLRC2*$^+$ NK had 177 downregulated and 37 upregulated genes as compared with *KLRC2*$^-$ cNK (figure 2D). Post-expansion, *KLRC2*$^+$ ADAPT-NK had 176 downregulated and 221 upregulated genes as compared with baseline *KLRC2*$^+$ adaptive NK (figure 2E). Consistent with published transcriptomes for adaptive NK cells,[23 34] baseline *KLRC2*$^+$ NK cells had higher expression of *LAG3*, *PROK2* and *MCOLN2* and lower expression of *FCER1G*, *IL12RB2*, *XCL2*, *CCNJL* and *SOX4* as compared with *KLRC2*$^-$ cNK. Postexpansion, *KLRC2*$^+$ ADAPT-NK cells showed upregulation of *FCER1G* and *IL12RB2* whereas expression of other adaptive signature genes was similar (figure 2F).

Next, the transcriptional signature with 397 differentially expressed (DE) genes for *KLRC2*$^+$ ADAPT-NK cells postexpansion (figure 2E) was interrogated. PPI analysis with the upregulated DE genes as a base resulted in a network of 208 elements (nodes; figure 2G), which was queried for pathway enrichment revealing lymphocyte activation and differentiation as highly upregulated processes (figure 2H, online supplemental sFigure 2C and online supplemental sTable 3). Using the downregulated DE genes as a base resulted in a network of 173 elements (nodes; figure 2I) where regulation of cell metabolism and proliferation dominated (figure 2J, online supplemental sFigure 2D and online supplemental sTable 4). Several DE genes annotated to cytokine-mediated signaling pathway and regulation of apoptosis were discovered among the observed downregulated and upregulated processes. Notably, despite a phenotypic resemblance to exhausted T cells,[35] cell exhaustion or senescence were not among the enriched processes and the overlap to transcriptional T cell exhaustion signatures was minimal (online supplemental sFigure 2E,F). Taken together, this reveals that expanded ADAPT-NK cells largely retained their adaptive state with evidence of metabolic and effector cell activation without signs of exhaustion.

ADAPT-NK cells are highly functional with predictable alloreactivity

To elucidate the functional capacity of the ADAPT-NK cells, we next explored responses to a range of stimuli. We observed strong ADCC against anti-CD20-coated 721.221 B-cell lymphoma targets but also robust IFN-γ production in response to IL-12/IL-18 stimulation (figure 3A,B), suggesting that ADAPT-NK cells retain an adaptive NK cell functional profile and, in addition, become more responsive to cytokine stimulation.[22 26–28] To investigate the contribution of signaling mediated via NKG2C/HLA-E interactions for ADAPT-NK cell functionality, expanded cells were tested against targets without HLA-E or engineered to express high levels of a β2m HLA-E single-chain trimer with forced presentation of the HLA-G leader peptide. K562 and NALM-6 target cells with high levels of HLA-E trimer elicited strong responses from ADAPT-NK cells above those of K562 wildtype (K562wt) or NALM-6 HLA-E KO, showing that the NKG2C receptor is signaling and contributes to the functional response of ADAPT-NK cells (figure 3C,D).

To test the HLA-Cspecificity of ADAPT-NK responses, expanded NKG2C$^+$KIR2DL1$^+$KIR2DL3$^-$ or KIR2DL3$^+$KIR2DL1$^-$ ADAPT-NK cells were stimulated with K562wt cells or K562 cells engineered to express high levels of single chain β2m HLA-C1 or HLA-C2 dimers. Strong responses were observed in the HLA-C/KIR mismatched setting but ADAPT-NK cells were inhibited in the matched setting (figure 3E,F and online supplemental sFigure 3A). In mixed target cell assays, ADAPT-NK cells preferentially killed HLA-C mismatched targets (figure 3G,H). Assessing the cytotoxic potential of individual NK cells in a microwell screening assay,[32] there were significantly more kills per cytotoxic cell in the HLA-C/KIR mismatched setting and enhanced serial killing ability (figure 3I–K). These results revealed that ADAPT-NK cells efficiently convert the HLA-E check point into an activation signal and show specific and predictable alloreactivity against K562 targets expressing high levels of mismatched HLA-C.

Efficient alloreactivity against tumor cell lines and in vivo efficacy of ADAPT-NK cells

The importance of alloreactivity for tumor targeting was apparent when assessing the ADAPT-NK cell product. We next tested the long-term killing ability against tumor cell lines of various HLA-C genotypes but overall low/negative for HLA-E (figure 4A–C and online supplemental sFigure 3B–F). A group of tumor lines displayed negligible expression of HLA-C and were subsequently killed equally well by HLA-C/KIR-matched and mismatched ADAPT-NK cells (online supplemental sFigure 3C–F). Two HLA-C2/C2 tumor lines, BJAB (Burkitt-like lymphoma) and HL-60 (AML), displayed significant levels of HLA-C2 as assessed by KIR2DL1-Fc binding, and high rates of killing could be observed in the mismatched setting (figure 4A–C).

To evaluate the in vivo impact of ADAPT-NK cell alloreactivity, NSG mice were injected with luciferase-tagged HL-60 cells followed by a flat dose of 5×10^6 HLA-C/KIR-matched or mismatched ADAPT-NK, under in vivo IL-15 support. The tumor burden was significantly reduced by ADAPT-NK cell transfer for the duration of the experiment, with substantially better leukemia control by HLA-C/KIR mismatched ADAPT-NK cells by day 35 (figure 4D,E). Together this demonstrates the therapeutic efficacy of alloreactive ADAPT-NK against HLA-C mismatched tumor cells and underscores their ability to deliver a maximized missing-self response in settings with high levels of mismatched HLA-C.

ADAPT-NK cells show potent alloreactivity against mismatched primary AML blasts and combination with an CD33/IL-15/CD16 TriKE overcomes resistant blast subtypes

Thus far, expanded ADAPT-NK cells showed efficient killing of tumor cell lines in vitro and in vivo. We next tested the ability of NKG2C$^+$KIR2DL1$^+$KIR2DL3$^-$ or KIR2DL3$^+$KIR2DL1$^-$ ADAPT-NK cells to recognize and

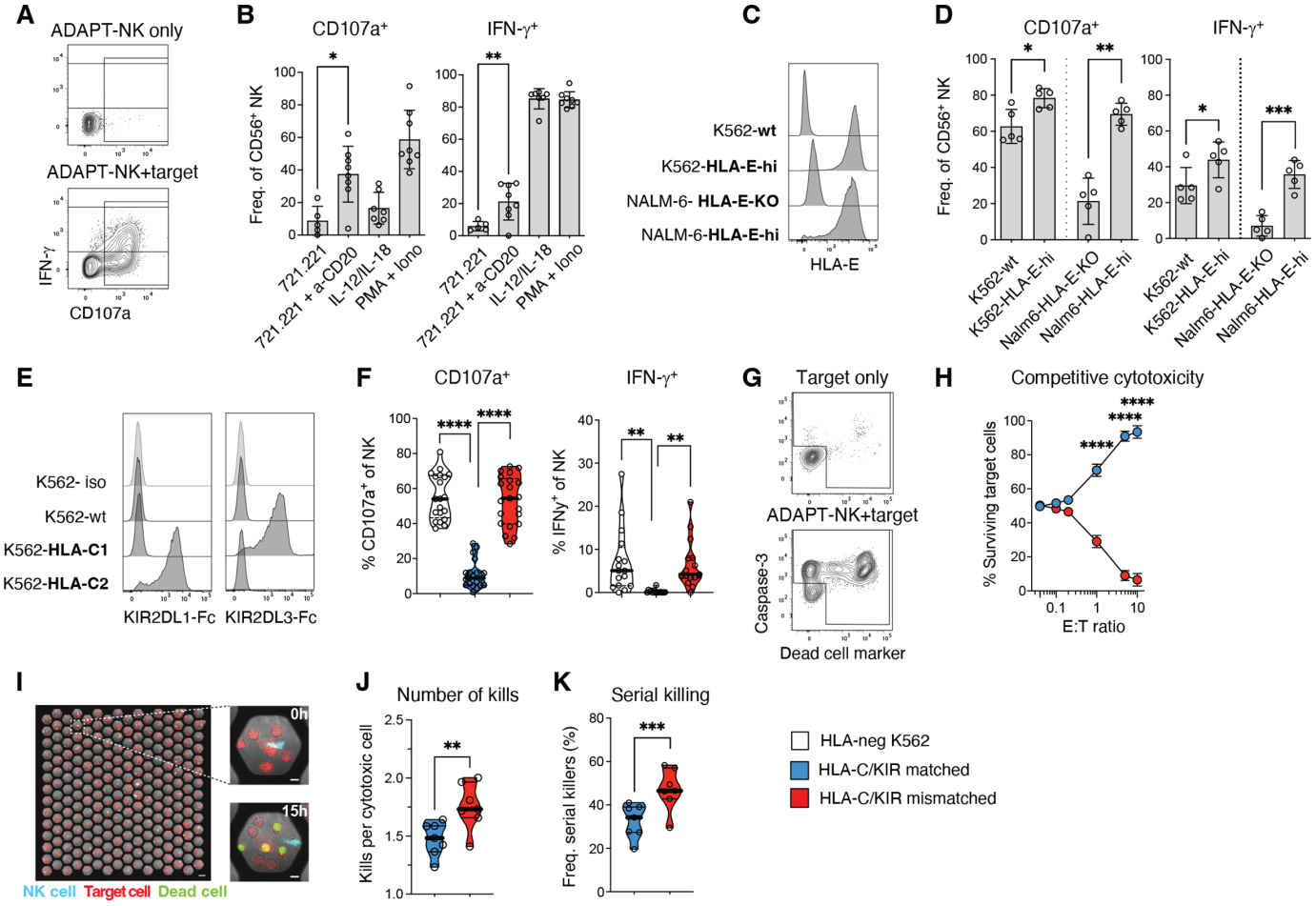

Figure 3 ADAPT-NK cells are highly functional with predictable alloreactivity. (A) Functional analysis of NK cells by flow cytometry in terms of degranulation (CD107a) and IFN-γ production. (B) ADAPT-NK responses to 721.221 target cells with or without anti-CD20 (MabThera) addition, and to IL-12+IL-18 or PMA+Ionomycin stimulation. (C, D) ADAPT-NK responses to K562 or NALM-6 tumor target cells with varying expression levels of HLA-E. (E) Determination of HLA-C expression by means of KIR-Fc staining for K562 engineered with single chain β2m HLA-C1 or HLA-C2 dimers. (F) Responses of KIR2DL1$^+$ KIR2DL3$^-$ KIR2DL2$^-$ NKG2A$^-$ or KIR2DL1$^-$ KIR2DL3$^+$ KIR2DL2$^-$ NKG2A$^-$ ADAPT-NK cells to HLA-C1 or HLA-C2 K562 in the HLA-C/KIR matched and mismatched setting. (G) Target cell death judged by Dead Cell Marker and caspase-3 staining to determine freq. of remaining live target cells. (H) Frequency of live target cells after mixed target cell assays with ADAPT-NK cells in the HLA-C/KIR matched and mismatched setting. (I–K) The cytotoxic potential of individual NK cells in the HLA-C/KIR matched and mismatched setting was assessed in a microwell screening assay. (J) Average number of kills performed by the cytotoxic NK cells. (K) Corresponding fraction of cytotoxic NK cells killing >1 target. For (B) n=8 in two independent experiments, (D) n=5 in one independent experiment, (F–H) n=11 in three independent experiments with KIR2DL1$^+$ and KIR2DL3$^+$ subsets analyzed in all donors, (I–K) n=7 in four independent experiments. Statistical differences were calculated using paired t-tests (in B, D, J–K) and a one-way ANOVA with Sidak's correction (F–H). *p<0.05, **p<0.01, ***p<0.001, p<0.0001. ANOVA, analysis of variance; KIR, killer immunoglobulin-like receptor; NK, natural killer; PMA, phorbol myristate acetate.

eliminate primary AML blasts in PBMC samples derived from patients with distinct HLA-C genotypes. Patient characteristics, including cytogenetics and HLA-C haplotypes, is displayed in online supplemental sFigure 4A. Corroborating the importance of NK cell alloreactivity, minimal NK cell cytotoxicity was observed in HLA-C/KIR matched conditions, whereas mismatched CD45^{dim} AML blasts were efficiently killed at different E:T ratios (figure 5A,B and online supplemental sFigure 4B). The killing of the AML blasts by mismatched ADAPT-NK cells was variable, with some patient samples being more effectively killed and others more resistant. Since the blast compartment of the different samples was heterogeneous, we could monitor putative immune selection events and resistant subtypes. No relation was found between specific cytotoxicity by mismatched ADAPT-NK cells and HLA-DR, CD33, CD34, CD38, CD47, CD112, CD117 or CD155 expression on CD45^{dim} blasts (online supplemental sFigure 4C). Detected levels of HLA-E on blasts were overall low but correlated with sensitivity to killing (figure 5C).

Lack of NKG2D ligand expression is associated with leukemic stem cells (LSC) and involved in mediating their immune evasion.[36] Although NKG2DL$^+$ blasts were eliminated to a higher extent, NKG2DL$^-$ LSC were still killed, even at low E:T ratios (figure 5D and online supplemental sFigure 4C). To increase killing of more resistant

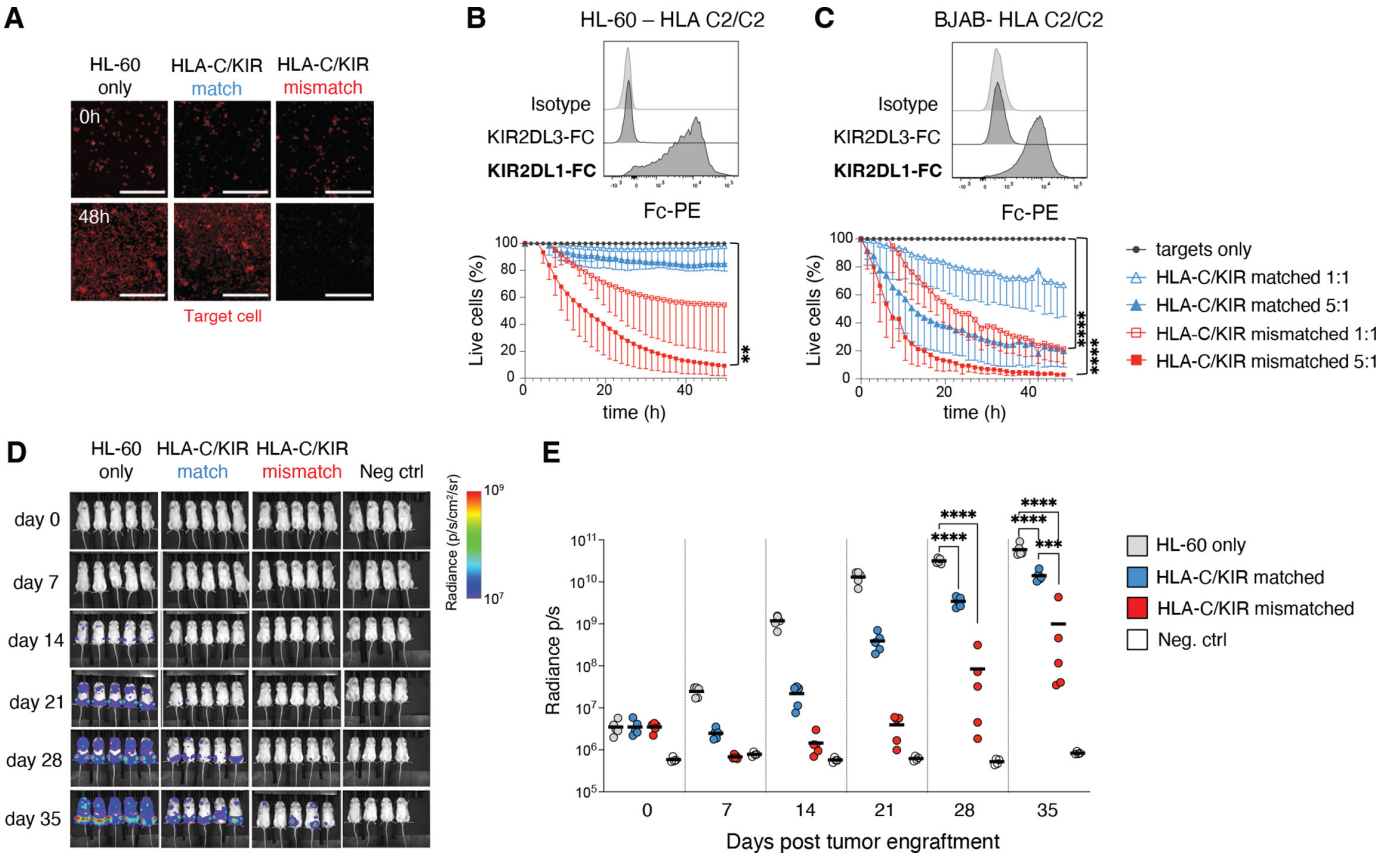

Figure 4 Efficient killing of HLA-C/KIR mismatched tumor cell lines and in vivo efficacy of expanded ADAPT-NK cells. (A–C) Determination of killing ability of ADAPT-NK cells over 48 hours against tumor cell lines of various HLA-C genotypes in the IncuCyte platform, in bold the expected KIR-Fc binding. n=4–9 donors, in at least two independent experiments for each target cell line. Data are displayed as mean (±SD) and significance is given between HLA-C/KIR mismatched and targets only. Scalebar represents 300 µM. (D) a representative example from two independent experiments of bioluminescence in NSG mice injected with luciferase tagged HL-60 4 days prior to injection with a flat-dose of HLA-C/KIR matched or mismatched ADAPT-NK cells and subsequent evaluation for 35 days, compiled data displayed as means in (E). Fifteen mice were used with n=2 ADAPT-NK cells. Four control mice were used. Statistical differences were tested using a one-way ANOVA with Sidak's correction (B, C) or a two-way ANOVA followed by Tukey's multiple comparison correction (E). *p<0.05, **p<0.01, ***p<0.001, ****p<0.0001. ANOVA, analysis of variance; KIR, killer immunoglobulin-like receptor; NK, natural killer.

blast subtypes, we combined mismatched ADAPT-NK cells with a CD16/IL-15/CD33 tri-specific engager (TriKE), previously used to target AML blasts.[37] The expression of CD33 on AML blasts was high and addition of the TriKE resulted in significantly improved killing of AML blasts, even for more resistant samples and NKG2DL$^-$ LSC (figure 5E,F and online supplemental sFigure 4C). Thus, ADAPT-NK cells showed high efficacy against primary AML blasts, and due to their strong ADCC capacity, such expanded adaptive NK cells can be combined with immune engagers to overcome partial NK cell resistance of LSC.

DISCUSSION

NK cell-based immunotherapy can be a safe and effective treatment for subgroups of leukemia patients with relapsed or refractory disease. Emerging therapeutic approaches focus on enhancing NK cell cytotoxicity and persistence in vivo and making the therapy more readily available in off-the-shelf strategies. One constituent of the NK antitumor response is alloreactive cells in administered NK cell products that relate to better clinical outcomes.[2 10 11] The preferential expression of a single self-KIR on most adaptive NK cells provides an opportunity to boost the alloreactive response through selective expansion of this NK subset. Adaptive NK cells also inherently display high ADCC capacity and enhanced IFN-γ production.[18 21 24 25] To harness these properties, we developed a single self-KIR$^+$NKG2C$^+$ adaptive NK cell product termed ADAPT-NK, using cryopreserved third-party donor material in a fully GMP-compliant protocol. Transcriptional signatures and adaptive features were largely preserved in ADAPT-NK cells post-expansion and the cells exhibited three natural functional modalities without genetic editing: Alloreactivity (single KIR), HLA-E targeting (NKG2C$^+$NKG2A$^-$) and potent ADCC activity (CD16 expression and signaling).

Generation of homogeneous alloreactive NK populations can theoretically be achieved through (1)

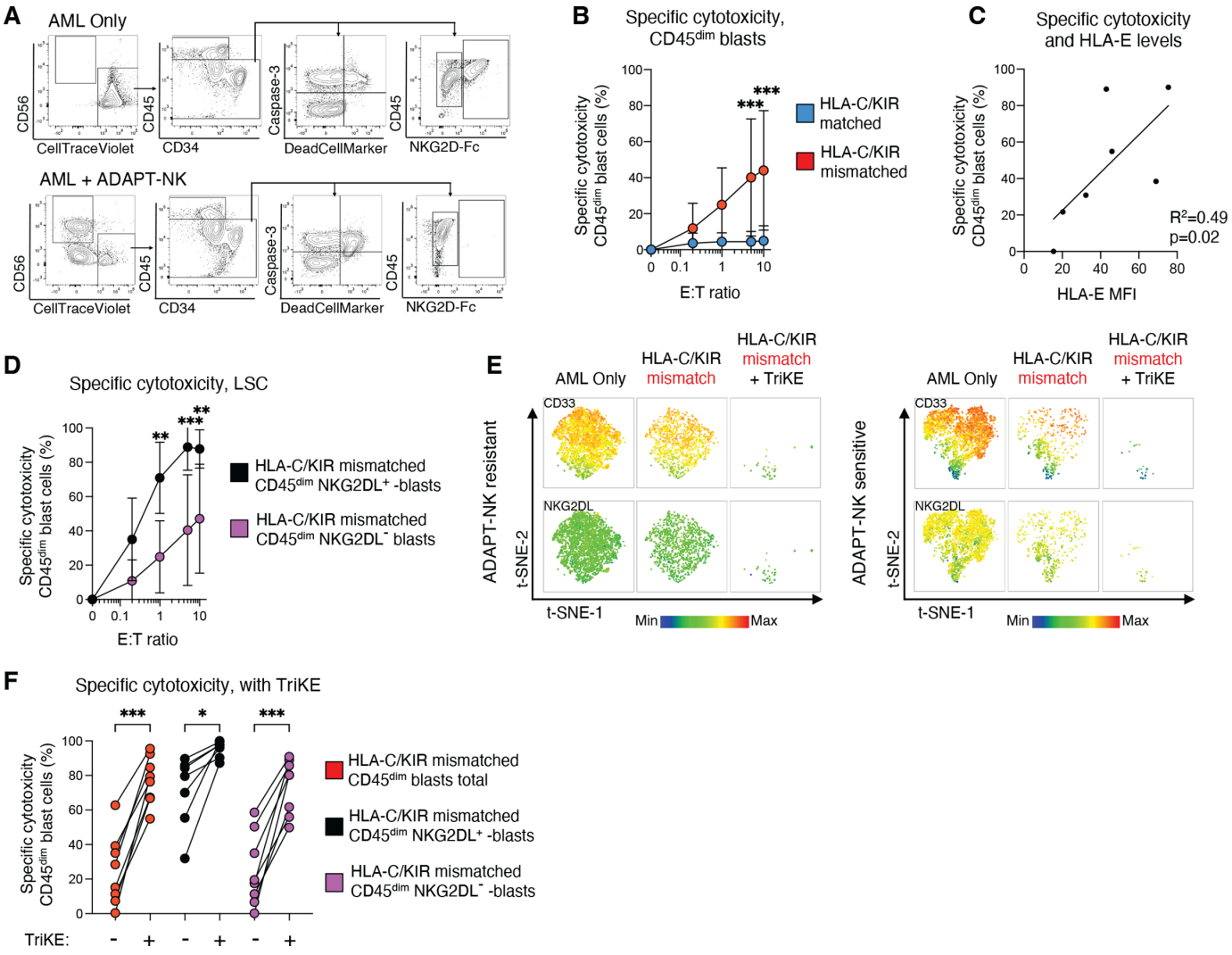

Figure 5 ADAPT-NK cells show potent and specific alloreactivity against mismatched primary AML blasts and combination with CD33/IL-15/CD16 TriKE overcomes resistant blast subtypes. (A) Gating strategy for phenotyping of primary AML blast cells ($CD45^{dim}$) by flow cytometry, as well as specific target cell killing calculated by the change in Dead Cell $Marker^{+}$ $Caspase\text{-}3^{+}$ target cells in co-cultures with ADAPT-NK cells. (B) Specific target cell cytotoxicity of AML blasts in HLA-C/KIR -matched and -mismatched conditions at different E:T ratios. (C) Spearman correlation between the mean specific cytotoxicity against each blast sample at 5:1 E:T ratio and the HLA-E expression on the corresponding $CD45^{dim}$ AML blasts. (D) Specific target cell killing of leukemic stem cells (LSC) ($NKG2DL^{-}$) and non-LSCs ($NKG2DL^{+}$) in HLA-C/KIR mismatched conditions at multiple E:T ratios. (E) t-SNE plot of ADAPT-NK sensitive and resistant AML samples co-cultured at 1:1 with HLA-C/KIR mismatched ADAPT-NK cells with and without the addition of CD33/IL-15/CD16 TriKE (TriKE). Heatmap overlays expression of CD33 (top row) and NKG2DL (bottom row). (F) Mean specific cytotoxicity of different blast subsets at 1:1 E:T ratio with or without the addition of TriKE. (A–F) Primary AML samples n=7 and ADAPT-NK products n=8 (overall 14 HLA-C/KIR-matched and 14 HLA-C/KIR-mismatched interactions) in three independent experiments. Statistical differences were tested using a two-way ANOVA followed by Sidak's multiple comparison correction (B, D), using Spearman's correlation (C) or using one-way ANOVA followed by Sidak's multiple comparison correction (F). *p<0.05, **p<0.01, ***p<0.001. AML, acute myeloid leukemia; ANOVA, analysis of variance; E:T, effector to target; KIR, killer immunoglobulin-like receptor; NK, natural killer; t-SNE, t-distributed stochastic neighbor embedding.

selection of single-KIR^{+} NK cells and subsequent expansion,[38] (2) guided differentiation of precursors with or without genetic editing or (3), as shown here, through selective outgrowth from a mixed NK cell population.[14] The selective expansion of adaptive NK cells from a mixed NK population avoids any need for GMP-grade selection or editing procedures and therefore reduces the complexity of culturing. Robust cell expansions were generated from all donors with large pre-existing $NKG2C^{+}$ adaptive NK cell subsets, recapitulating the NKG2C phenotype with only slight variation in replicate experiments. This included those donors with almost exclusively $CD57^{+}NKG2C^{+}$ adaptive NK cells pre-expansion, suggesting that proliferation could be induced in this subset despite the low proliferative capacity of CD57-expressing cells.[39]

Of note, and in contrast to many cytokine-driven expansion protocols, there was no increase in the

fraction of cells expressing NKG2A. In fact, NKG2A expression on NKG2C$^+$ ADAPT-NK cells was negligible, resembling NK cell preparations generated by CRISPR editing[40] or through intracellular retention.[41] The NKG2A expression remained low also during the phase of intense proliferation coinciding with the disappearance of HLA-E expressing feeders around day 7, suggesting an inheritable adaptive state. Absence of NKG2A-mediated inhibition with concomitant homogeneous expression of NKG2C on ADAPT-NK cells allowed for efficient reactivity toward HLA-E-expressing targets. Hence, in addition to KIR-driven alloreactivity, the switched HLA-E recognition enables targeting of tumors with high HLA-E levels where NKG2A otherwise provides an inhibitory check point.[42]

Adaptive NK cells have a distinct molecular signature including alterations in signaling molecules and surface receptors.[18 22 23] Transcriptional analysis revealed that although *FCER1G* and *IL12RB* were upregulated the adaptive imprint was largely intact post ADAPT-NK cell expansion. Notably, CD16 and co-stimulatory CD2 expression, critical for the superior ability of adaptive NK cells to respond to antibody-coated target cells,[33] remained high enabling potent ADCC responses with rituximab and the CD16-IL-15-CD33 TriKE.

Lack of inhibitory input from tumor targets led to ADAPT-NK cell attack in HLA-C/KIR mismatched settings whereas tolerance to self was maintained in matched settings with high HLA-C expression. In addition to NKG2C, the cells displayed high levels of NKG2D, upregulated NKp30 and maintained DNAM-1 levels. They also displayed high levels of effector enzymes such as Granzyme B and perforin, above those of conventional NK cells. Overall, the ADAPT-NK cells showed upregulation of receptors and enrichment of genes related to activation, differentiation, proliferation, cytokine signaling, and regulation of apoptosis and metabolism. Although ADAPT-NK cells expressed surface markers classically associated with T cell exhaustion such as TIM-3, LAG-1 and TIGIT, the transcriptional overlap to exhausted CAR T cells was minimal and did not include the signature marker TOX.[43 44] Exhaustion in the NK cell compartment is still not well defined. The role of PD-1 on NK cells is controversial and TIGIT and TIM-3 may correlate both with activation/acute stimulation and more exhausted states.[45] Most importantly, the ADAPT-NK cells showed potent proliferation and cytotoxicity, also in longer-term in vitro assays and displayed serial killing capacity, demonstrating that they were not functionally exhausted.

AML is a heterogeneous disease with varying blast presentations and subtypes. ADAPT-NK cells were highly efficient against an AML cell line in vitro and in vivo as well as against primary AML blasts. Following a single dose of KIR-L mismatched ADAPT-NK cells, tumor burden was significantly reduced in the HL-60 AML mouse model with superior early limitation of tumor growth. Although this in vivo model is extensively used to assess NK cell function,[37 46] a weakness of the model is the aggressive nature of the tumor with exponential growth as soon as the tumor escapes initial control, which precludes comprehensive survival analyses.

Against primary patient blasts, efficacy of mismatched ADAPT-NK killing was correlated to HLA-E expression on CD45^{dim} blasts as well as NKG2D-L expression and varied greatly among samples. Previous studies have identified the NKG2DL$^-$ blasts as particularly NK resistant and able to give rise to new blast populations acting as LSCs.[36] Therefore, it was particularly important to observe the killing of NKG2DL$^-$ blasts even without stimulatory NKG2D input, and an enhanced effect with the TriKE immune engager. This was evident also for blasts carrying poor-prognosis mutations such as FLT3-ITD.[47] More extensive studies are needed to elucidate resistant and susceptible AML subtypes, also considering the genetic makeup of the AML clone(s), to enable patient stratification in a precision immunotherapy pipeline.

Beneficial features of adaptive NK cells are currently under development from third-party donor cells and engineered iPSC NK cells, mainly focused on NKG2C, FcεRIγ, and CD38 negativity in combination with daratumumab for multiple myeloma.[48 49] Like the 'g-NK cells',[48] ADAPT-NK cells circumvent the need for genetic engineering while relying on preselection of donors harboring adaptive NK subpopulations. Our KIR-centered strategy meant sourcing donors with adaptive NK cells educated by self-KIR2DL1 (HLA-C2/C2 or HLA-C1/C2) or -KIR2DL3 (HLA-C1/C1 or HLA-C1/C2), intended for treating patients with homozygous HLA-C1 or -C2 haplotypes. In preparation for a phase I/II clinical trial for refractory leukemias, we have established a GMP-grade donor cell bank with cryopreserved CD3/CD19 depleted apheresis products from so far nine superdonors (recruitment ongoing), sufficient to manufacture 350 ADAPT-NK doses in an off-the-shelf setting. Although a complete KIR-L mismatch would be the most appealing approach, there is a risk for off-target cytotoxic effects, necessitating precautions in initial dosing regimens. Another important point to consider is the risk for downtuning (or disarming) of NK cell function following adoptive transfer to an HLA disparate recipient, as has been shown in MHC-deficient mice.[50]

In summary, by expanding adaptive single-self-KIR$^+$ NKG2C$^+$ NK cells in a fully scalable GMP-compliant protocol our study provides the basis to explore alloreactive NK cell therapy. We see potential implications for combination therapies where the ADAPT-NK cell therapy platform is combined with immune engagers or engineering with CARs. If successful, clinical trials based on the ADAPT-NK cells may be able to answer

fundamental questions regarding the importance of alloreactivity for GvL effects in hematological malignancies.

Author affiliations
[1]Center for Infectious Medicine, Department of Medicine Huddinge, Karolinska Institutet, Stockholm, Sweden
[2]Department of Cancer Immunology, Institute for Cancer Research, Oslo University Hospital and University of Oslo, Oslo, Norway
[3]Department of Applied Physics, Science for Life Laboratory, KTH Royal Institute of Technology, Stockholm, Sweden
[4]University of Minnesota, Masonic Cancer Center, Minneapolis, Minnesota, USA
[5]Department of Hematology, Oslo University Hospital and K.G. Jebsen Centre for B-cell malignancies, Institute of Clinical Medicine, University of Oslo, Oslo, Norway
[6]Vecura, Karolinska Center for Cell Therapy Clinical Research Center, Karolinska University Hospital, Stockholm, Sweden
[7]Center for Hematology and Regenerative Medicine, Department of Medicine Huddinge, Karolinska Institutet, Stockholm, Sweden
[8]Department of Microbiology, Tumour and Cell Biology, Karolinska Institutet, Stockholm, Sweden
[9]Department of Clinical Immunology and Transfusion Medicine, Karolinska University Hospital, Stockholm, Sweden
[10]Fate Therapeutics Inc, La Jolla, California, USA
[11]Department of Cellular Therapy and Allogeneic Stem Cell Transplantation, Karolinska University Hospital, Stockholm, Sweden

Correction notice This article has been updated since it was first published online. The paragraph under the heading 'ADAPT-NK cell expansion protocol' has been updated to include the sentence '10% human ab serum (TCS Biosciences or Access Biologicals), 2mM L-glutamine (Cytiva -FisherScientific)'.

Twitter Karl-Johan Malmberg @MalmbergLab

Acknowledgements We thank all blood and leukapheresis donors and the staff at the blood bank and leukapheresis unit. Also, a special thanks to research nurse Josephine Johansson for excellent and dedicated help with donor identification and handling. CITE-Seq experiments were performed by the Genetics core facility at Oslo University Hospital. Biorender.com was used to create some figure elements.

Contributors A.H-I, MV, HN, HVO, BZ, LB, PM, MK, MW, SL, HJH, SB, VK, SZK, QH and ES conducted experiments and analyzed data. KW and PB provided technical assistance. BV, GT, PH and MF provided critical reagents or patient samples. EHL, BO, EA, H-GL, AB, LK, FC, and JM provided scientific input. ES, K-JM. and AH-I designed the research and wrote the manuscript with edits from all authors K-JM acts as guarantor of the work presented here.

Funding This work was supported by grants from the Swedish Research Council (223310), the Swedish Children's Cancer Society (PR2020-1059), the Swedish Cancer Society (21-1793Pj), Sweden's Innovation Agency, the Karolinska Institutet, the Norwegian Research Council (275469). The South-Eastern Norway Regional Health Authority (2021-073), the Norwegian Cancer Society (223310), European Commission H2020-MSC-ITN-765104-MATURE-NK, the EU's Horizon 2020 Marie Skłodowska-Curie Actions (MSCA 838909), Knut and Alice Wallenberg Foundation, Swedish Foundation for Strategic Research, the US National Cancer Institute P01 CA111412 (JSM, FC, K-JM) and Fate Therapeutics.

Competing interests K-JM is a consultant with ownership interests at Fate Therapeutics and Vycellix and has research funding from Fate Therapeutics. He has a Royalty agreement with FATE Therapeutics through licensing of IP. K-JM has received honoraria from Oncopeptides, Cytovia and has research funding from Oncopeptides and Merck. ES is a paid consultant at Fate Therapeutics. H-GL is a founder and serves on the board of XNK Therapeutics and Vycellix. He has a Royalty agreement with FATE Therapeutics through licensing of IP. EA is a founder of XNK therapeutics, Vycellix, VyGenBio and Fuse therapeutics. EA also serves as an advisor to Artiva, Avectas, Virocell, and Sorrento therapeutics. All relationships have been reviewed and managed by Oslo University Hospital and Karolinska Institute in accordance with its conflict-of-interest policies. BV is an employee of Fate Therapeutics. BÖ is a consultant and has ownership interests at Vycellix and has research funding from Affimed. FC and JSM are paid consultants to, and receive research funds from, Fate Therapeutics. JSM serves on the Scientific Advisory Board of OnkImmune, Nektar, Magenta and is a paid consultant consult for GT BioPharma and Vycellix.

Patient consent for publication Not applicable.

Ethics approval The study was approved by the Swedish Ethical Review Authority, Sweden (Dnr 2020-05289 and Dnr 2019-02657)], Regional committees for Medical and Health Research Ethics in Norway, REK Sør-Øst, (Biobank ID 2012/1143 and project ID 2015/2142). The studies were conducted in accordance with the Declaration of Helsinki. All blood donors and AML patients provided written consent for collection of samples and biobank storage. Participants gave informed consent to participate in the study before taking part.

Provenance and peer review Not commissioned; externally peer reviewed.

Data availability statement Data are available in a public, open access repository. RNA Sequencing data is available at EMBL-EBI European Nucleotide Archive, EGAX. The count matrices have been deposited in the ArrayExpress database under accession number E-MTAB-12228. The raw sequencing data have been deposited to EGA under accession number EGAS00001006614.

ORCID iDs
Alvaro Haroun-Izquierdo http://orcid.org/0000-0003-4557-3606
Marianna Vincenti http://orcid.org/0000-0001-5361-0185
Herman Netskar http://orcid.org/0000-0002-3081-9581
Minoru Kanaya http://orcid.org/0000-0002-0035-8657
Martin Felices http://orcid.org/0000-0002-5945-0634
Lise Kveberg http://orcid.org/0000-0001-9308-0641
Karl-Johan Malmberg http://orcid.org/0000-0002-8718-9373
Ebba Sohlberg http://orcid.org/0000-0003-1942-0040

REFERENCES

1 Miller JS, Soignier Y, Panoskaltsis-Mortari A, *et al*. Successful adoptive transfer and in vivo expansion of human haploidentical NK cells in patients with cancer. *Blood* 2005;105:3051–7.
2 Curti A, Ruggeri L, D'Addio A, *et al*. Successful transfer of alloreactive haploidentical Kir ligand-mismatched natural killer cells after infusion in elderly high risk acute myeloid leukemia patients. *Blood* 2011;118:3273–9.
3 Romee R, Rosario M, Berrien-Elliott MM, *et al*. Cytokine-Induced memory-like natural killer cells exhibit enhanced responses against myeloid leukemia. *Sci Transl Med* 2016;8:ra123.
4 Ciurea SO, Schafer JR, Bassett R, *et al*. Phase 1 clinical trial using mbIL21 ex vivo-expanded donor-derived NK cells after haploidentical transplantation. *Blood* 2017;130:1857–68.
5 Björklund AT, Carlsten M, Sohlberg E, *et al*. Complete remission with reduction of high-risk clones following haploidentical NK-cell therapy against MDS and AML. *Clin Cancer Res* 2018;24:1834–44.
6 Myers JA, Miller JS. Exploring the NK cell platform for cancer immunotherapy. *Nat Rev Clin Oncol* 2021;18:85–100.
7 Horowitz A, Strauss-Albee DM, Leipold M, *et al*. Genetic and environmental determinants of human NK cell diversity revealed by mass cytometry. *Sci Transl Med* 2013;5:ra145.
8 Ljunggren HG, Kärre K. In search of the 'missing self': MHC molecules and NK cell recognition. *Immunol Today* 1990;11:237–44.
9 Kärre K. Immunology. A perfect mismatch. *Science* 2002;295:2029–31.
10 Ruggeri L, Capanni M, Urbani E, *et al*. Effectiveness of donor natural killer cell alloreactivity in mismatched hematopoietic transplants. *Science* 2002;295:2097–100.
11 Ruggeri L, Mancusi A, Burchielli E, *et al*. Natural killer cell alloreactivity in allogeneic hematopoietic transplantation. *Curr Opin Oncol* 2007;19:142–7.

12 Fauriat C, Andersson S, Björklund AT, *et al*. Estimation of the size of the alloreactive NK cell repertoire: studies in individuals homozygous for the group A Kir haplotype. *J Immunol* 2008;181:6010–9.
13 Yawata M, Yawata N, Draghi M, *et al*. MHC class I-specific inhibitory receptors and their ligands structure diverse human NK-cell repertoires toward a balance of missing self-response. *Blood* 2008;112:2369–80.
14 Liu LL, Pfefferle A, Yi Sheng VO, *et al*. Harnessing adaptive natural killer cells in cancer immunotherapy. *Mol Oncol* 2015;9:1904–17.
15 Gumá M, Angulo A, Vilches C, *et al*. Imprint of human cytomegalovirus infection on the NK cell receptor repertoire. *Blood* 2004;104:3664–71.
16 Lopez-Vergès S, Milush JM, Schwartz BS, *et al*. Expansion of a unique CD57^{+}NKG2Chi natural killer cell subset during acute human cytomegalovirus infection. *Proc Natl Acad Sci U S A* 2011;108:14725–32.
17 Gumá M, Budt M, Sáez A, *et al*. Expansion of CD94/NKG2C+ NK cells in response to human cytomegalovirus-infected fibroblasts. *Blood* 2006;107:3624–31.
18 Béziat V, Liu LL, Malmberg J-A, *et al*. NK cell responses to cytomegalovirus infection lead to stable imprints in the human Kir repertoire and involve activating KIRs. *Blood* 2013;121:2678–88.
19 Rölle A, Pollmann J, Ewen E-M, *et al*. IL-12-producing monocytes and HLA-E control HCMV-driven NKG2C+ NK cell expansion. *J Clin Invest* 2014;124:5305–16.
20 Hammer Q, Rückert T, Borst EM, *et al*. Peptide-specific recognition of human cytomegalovirus strains controls adaptive natural killer cells. *Nat Immunol* 2018;19:453–63.
21 Luetke-Eversloh M, Hammer Q, Durek P, *et al*. Human cytomegalovirus drives epigenetic imprinting of the IFNG locus in NKG2Chi natural killer cells. *PLoS Pathog* 2014;10:e1004441.
22 Schlums H, Cichocki F, Tesi B, *et al*. Cytomegalovirus infection drives adaptive epigenetic diversification of NK cells with altered signaling and effector function. *Immunity* 2015;42:443–56.
23 Holmes TD, Pandey RV, Helm EY, *et al*. The transcription factor Bcl11b promotes both canonical and adaptive NK cell differentiation. *Sci Immunol* 2021;6:eabc9801.
24 Zhang T, Scott JM, Hwang I, *et al*. Cutting edge: antibody-dependent memory-like NK cells distinguished by FcRγ deficiency. *J Immunol* 2013;190:1402–6.
25 Luetke-Eversloh M, Killig M, Romagnani C. Signatures of human NK cell development and terminal differentiation. *Front Immunol* 2013;4:499.
26 Cichocki F, Cooley S, Davis Z, *et al*. CD56dimCD57+NKG2C+ NK cell expansion is associated with reduced leukemia relapse after reduced intensity hCT. *Leukemia* 2016;30:456–63.
27 Takenaka K, Nishida T, Asano-Mori Y, *et al*. Cytomegalovirus reactivation after allogeneic hematopoietic stem cell transplantation is associated with a reduced risk of relapse in patients with acute myeloid leukemia who survived to day 100 after transplantation: the Japan Society for hematopoietic cell transplantation Transplantation-related complication Working group. *Biol Blood Marrow Transplant* 2015;21:2008–16.
28 Green ML, Leisenring WM, Xie H, *et al*. Cmv reactivation after allogeneic hCT and relapse risk: evidence for early protection in acute myeloid leukemia. *Blood* 2013;122:1316–24.
29 Elmaagacli AH, Steckel NK, Koldehoff M, *et al*. Early human cytomegalovirus replication after transplantation is associated with a decreased relapse risk: evidence for a putative virus-versus-leukemia effect in acute myeloid leukemia patients. *Blood* 2011;118:1402–12.
30 Liu LL, Béziat V, Oei VYS, *et al*. *Ex Vivo* Expanded Adaptive NK Cells Effectively Kill Primary Acute Lymphoblastic Leukemia Cells. *Cancer Immunol Res* 2017;5:654–65.
31 Basha O, Shpringer R, Argov CM, *et al*. The DifferentialNet database of differential protein-protein interactions in human tissues. *Nucleic Acids Res* 2018;46:D522–6.
32 Guldevall K, Brandt L, Forslund E, *et al*. Microchip screening platform for single cell assessment of NK cell cytotoxicity. *Front Immunol* 2016;7:119.
33 Liu LL, Landskron J, Ask EH, *et al*. Critical role of CD2 co-stimulation in adaptive natural killer cell responses revealed in NKG2C-Deficient humans. *Cell Rep* 2016;15:1088–99.
34 Collins PL, Cella M, Porter SI, *et al*. Gene regulatory programs conferring phenotypic identities to human NK cells. *Cell* 2019;176:348–60.
35 Blank CU, Haining WN, Held W, *et al*. Defining 'T cell exhaustion'. *Nat Rev Immunol* 2019;19:665–74.
36 Paczulla AM, Rothfelder K, Raffel S, *et al*. Absence of NKG2D ligands defines leukaemia stem cells and mediates their immune evasion. *Nature* 2019;572:254–9.
37 Vallera DA, Felices M, McElmurry R, *et al*. Il15 trispecific killer Engagers (TriKE) make natural killer cells specific to CD33+ targets while also inducing persistence, in vivo expansion, and enhanced function. *Clin Cancer Res* 2016;22:3440–50.
38 Siegler U, Meyer-Monard S, Jörger S, *et al*. Good manufacturing practice-compliant cell sorting and large-scale expansion of single KIR-positive alloreactive human natural killer cells for multiple infusions to leukemia patients. *Cytotherapy* 2010;12:750–63.
39 Björkström NK, Riese P, Heuts F, *et al*. Expression patterns of NKG2A, Kir, and CD57 define a process of CD56dim NK-cell differentiation uncoupled from NK-cell education. *Blood* 2010;116:3853–64.
40 Berrien-Elliott MM, Cashen AF, Cubitt CC, *et al*. Multidimensional analyses of donor Memory-Like NK cells reveal new associations with response after adoptive immunotherapy for leukemia. *Cancer Discov* 2020;10:1854–71.
41 Kamiya T, Seow SV, Wong D, *et al*. Blocking expression of inhibitory receptor NKG2A overcomes tumor resistance to NK cells. *J Clin Invest* 2019;129:2094–106.
42 van Hall T, André P, Horowitz A, *et al*. Monalizumab: inhibiting the novel immune checkpoint NKG2A. *J Immunother Cancer* 2019;7:263.
43 Alfei F, Kanev K, Hofmann M, *et al*. Tox reinforces the phenotype and longevity of exhausted T cells in chronic viral infection. *Nature* 2019;571:265–9.
44 Marotel M, Villard M, Drouillard A, *et al*. Peripheral natural killer cells in chronic hepatitis B patients display multiple molecular features of T cell exhaustion. *Elife* 2021;10:e60095.
45 Judge SJ, Murphy WJ, Canter RJ. Characterizing the dysfunctional NK cell: assessing the clinical relevance of exhaustion, anergy, and senescence. *Front Cell Infect Microbiol* 2020;10:49.
46 Felices M, Lenvik TR, Kodal B, *et al*. Potent cytolytic activity and specific IL15 delivery in a second-generation trispecific killer Engager. *Cancer Immunol Res* 2020;8:1139–49.
47 Daver N, Schlenk RF, Russell NH, *et al*. Targeting FLT3 mutations in AML: review of current knowledge and evidence. *Leukemia* 2019;33:299–312.
48 Bigley AB, Spade S, Agha NH, *et al*. FcεRIγ-negative NK cells persist in vivo and enhance efficacy of therapeutic monoclonal antibodies in multiple myeloma. *Blood Adv* 2021;5:3021–31.
49 Woan KV, Kim H, Bjordahl R, *et al*. Harnessing features of adaptive NK cells to generate iPSC-derived NK cells for enhanced immunotherapy. *Cell Stem Cell* 2021;28:2062–75.
50 Joncker NT, Shifrin N, Delebecque F, *et al*. Mature natural killer cells reset their responsiveness when exposed to an altered MHC environment. *J Exp Med* 2010;207:2065–72.

Correction: *Adaptive single-KIR^{+}NKG2C^{+} NK cells expanded from select superdonors show potent missing-self reactivity and efficiently control HLA-mismatched acute myeloid leukemia*

Haroun-Izquierdo A, Vincenti M, Netskar H, *et al*. Adaptive single-KIR+NKG2C+ NK cells expanded from select superdonors show potent missing-self reactivity and efficiently control HLA-mismatched acute myeloid leukemia. *J Immunother Cancer* 2022;10:e005577. doi: 10.1136/jitc-2022-005577

This article has been updated since it was first published online. The paragraph under the heading 'ADAPT-NK cell expansion protocol' has been updated to include the sentence '10% human ab serum (TCS Biosciences or Access Biologicals), 2mM L-glutamine (Cytiva-FisherScientific)'.

J Immunother Cancer 2023;**11**:e005577corr1. doi:10.1136/jitc-2022-005577corr1

Haroun-Izquierdo et al, Supplemental Material

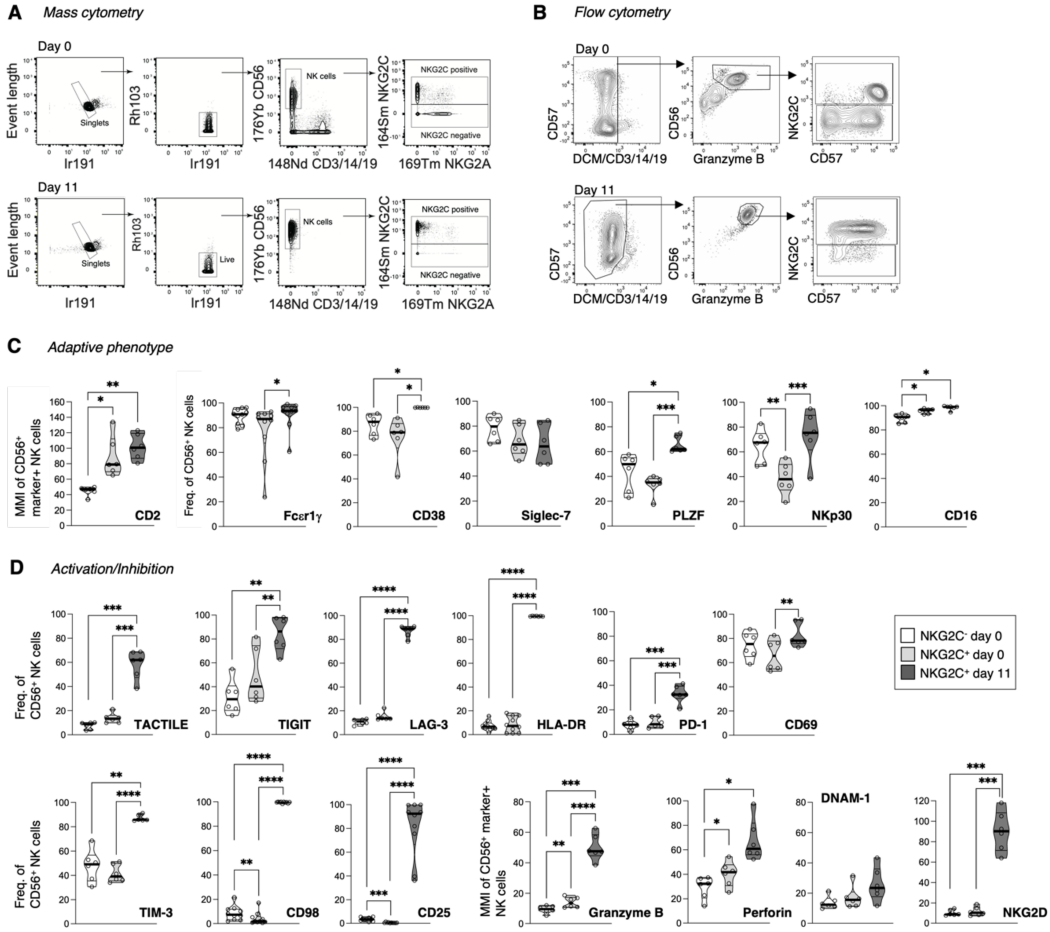

Supplemental Figure 1. Extended phenotyping by flow- and mass cytometry of ADAPT-NK cells. **A)** Gating scheme for mass cytometry analysis of NKG2C^{+} and NKG2C^{-} CD56^{+} NK cells. **B)** Gating scheme for flow cytometry analysis of NKG2C^{+} and NKG2C^{-} CD56^{+} NK cells, gated upstream on fsc-h/a and ssc-h/a single cells. **C-D)** Summary data that are the basis of heatmaps in Fig. 2B, frequencies of marker expression or mean metal intensity (MMI). Data for Fcεr1γ, HLA-DR, CD98 and CD25 derive from flow cytometry data. p-value <0.05 * <0.01 ** <0.001 *** <0.0001 **** in one-way ANOVA with Tukey's correction (C-D). For flow- and mass cytometry n=4-7.

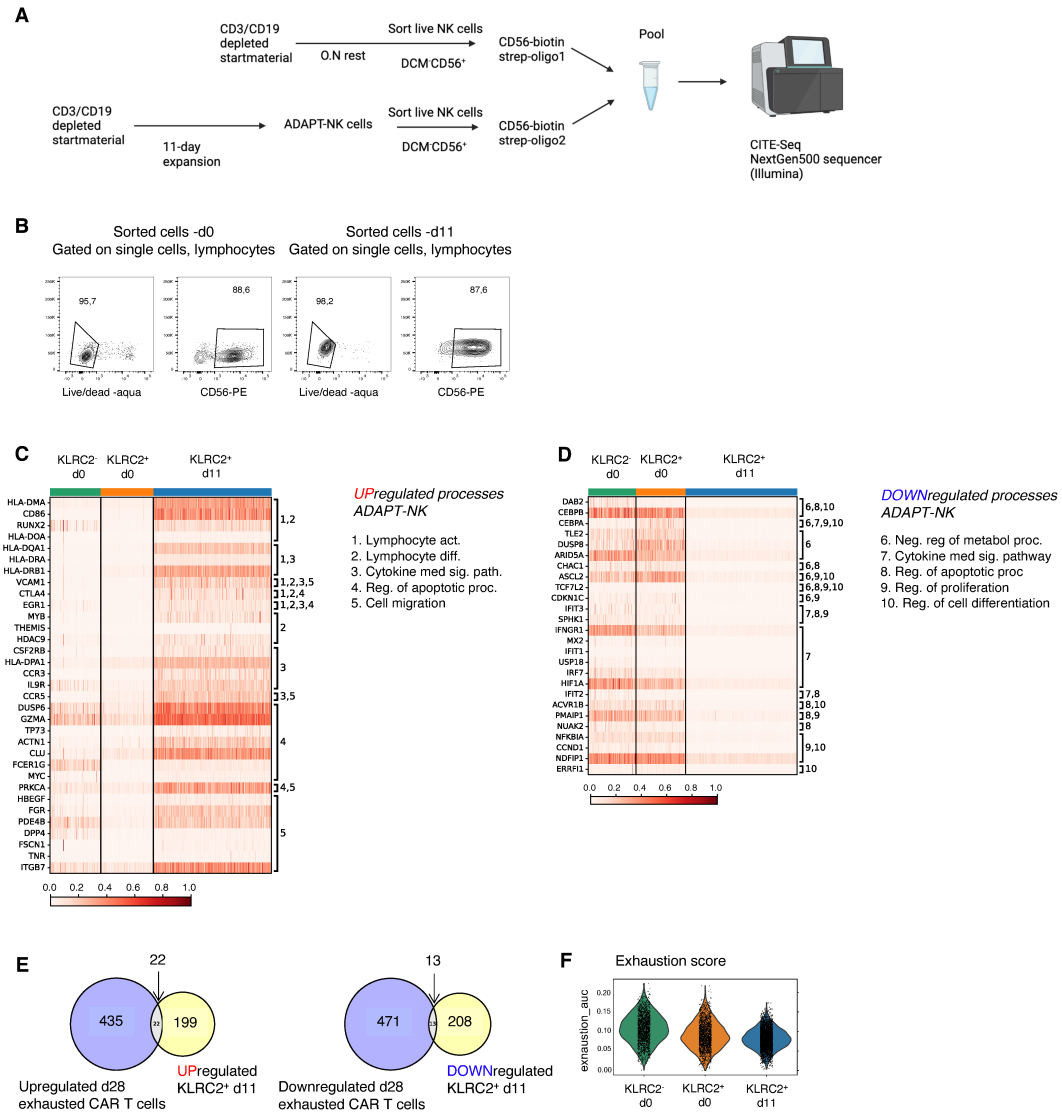

Supplemental Figure 2. ADAPT-NK cells show a retained adaptive transcriptional signature with activation of effector programs. A) CITE-Seq workflow **B)** Sort gates for day 0 and day 11 NK cells **C-D)** Heatmaps showing the expression of the upregulated **(C)** and downregulated (**D**) genes in ADAPT-NK in the CITE-seq data sorted by the identified clusters and showing the GO (BP) processes associated with these genes **E)** Venn diagram showing the overlap between the up- and down-regulated genes in the KLRC2^{+} day 11 cluster and up- and down-regulated genes in exhausted CAR T cells (Good et al., [1]). **F)** Exhaustion score computed using AUCell showing the activity of this signature in the clusters. CITE-Seq n=1.

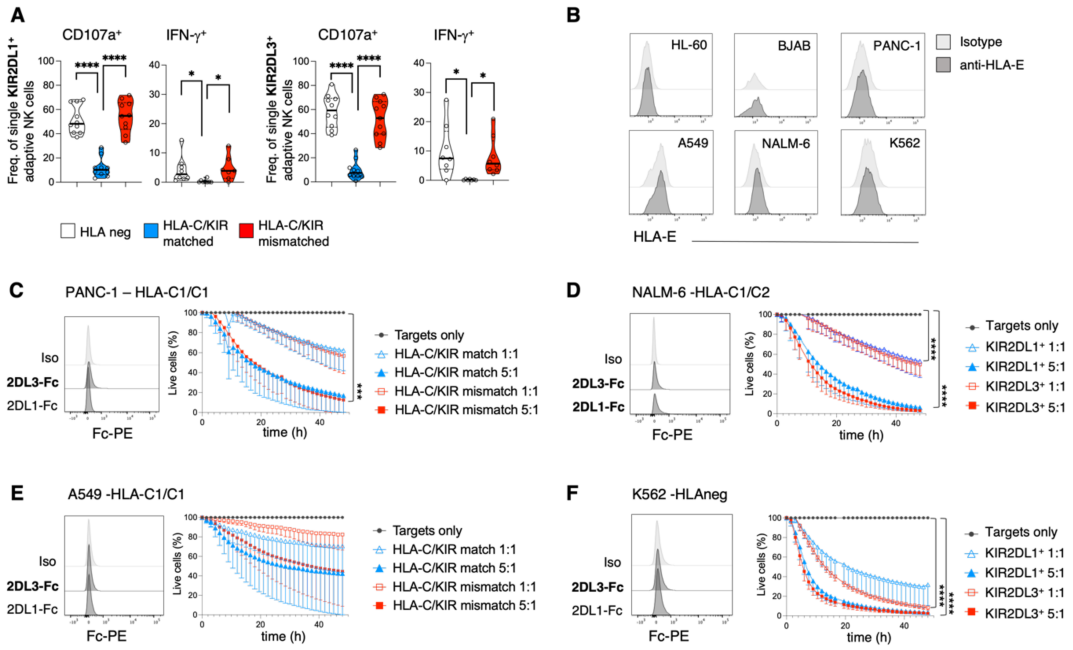

Supplemental Figure 3. ADAPT-NK cells are highly functional with predictable alloreactivity. Functional analysis of NK cells by flow cytometry in terms of degranulation (CD107a) and IFN-γ production. **A)** Responses of NKG2C$^+$ KIR2DL1$^+$ KIR2DL3$^-$ KIR2DL2$^-$ NKG2A$^-$ or NKG2C$^+$ KIR2DL1$^-$ KIR2DL3$^+$ KIR2DL2$^-$ NKG2A$^-$ ADAPT-NK cells to K562 with single chain β2m HLA-C1 or HLA-C2 dimers, in the HLA-C/KIR matched and mismatched setting. n=5-11, in 3 independent experiments with KIR2DL1$^+$ and KIR2DL3$^+$ subsets analyzed in all donors. **B)** Determination of HLA-E expression on tumor target lines. **C-F)** Determination of killing ability of ADAPT-NK cells over 48 h against tumor cell lines of various HLA-C genotypes and at different effector to target ratios (1:1 and 5:1) in the IncuCyte platform. In bold the expected KIR-Fc binding. n=4-9 donors, in at least two independent experiments for each target cell line. Data is displayed as mean (± SD) and significance is given between HLA-C/KIR mismatched and targets only. p-value <0.05 * <0.01 ** <0.001 *** <0.0001 **** in one-way ANOVA followed by Sidak's multiple comparison correction (C-F).

A

Patient sample	Diagnosis	Mutation	HLA-C
AML#1	AML	FLT3-ITD	C1/C1
AML#2	AML	no data	C1/C1
AML#3	AML	no data	C1/C1
AML#4	AML	FLT3-ITD	C2/C2
AML#5	AML	CEBP	C2/C2
AML#6	AML	FLT3-ITD	C1/C1
AML#7	AML	no data	C1/C1
AML#8	AML	NPMI1	C2/C2

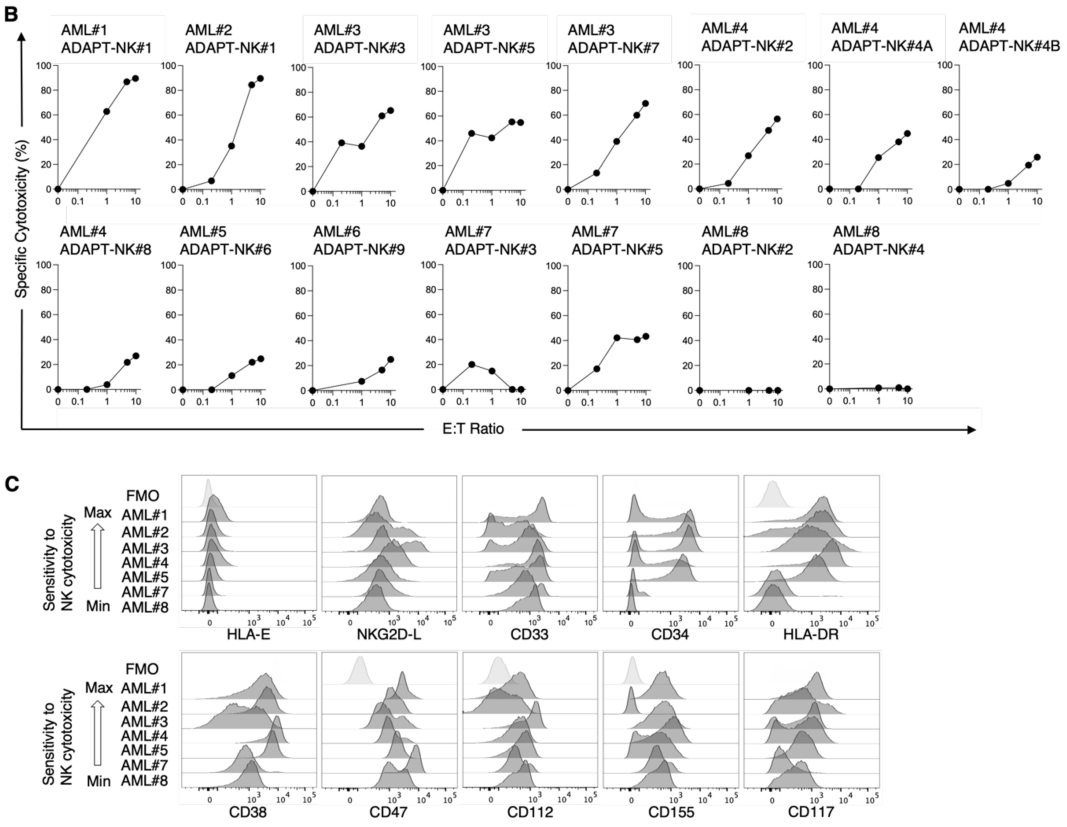

Supplemental Figure 4. Cytotoxicity of ADAPT-NK cells against primary AML blasts. A) AML patient cytogenetics and HLA-C haplotypes. **B)** Cytotoxicity against 8 primary AML blasts by 9 different HLA-C/KIR-mismatched ADAPT-NK products in 3 independent experiments. Some AML samples were co-cultured with multiple NK products (up to 3) in separate experiments. A and B notation on ADAPT-NK#4 denotes a repeat combination in 2 independent experiments. **C)** Surface marker expression of indicated proteins evaluated by flow cytometry on 7 $CD45^{dim}$ AML blasts and ordered based on decreased sensitivity to ADAPT-NK cell cytotoxicity, FMO – fluorescence minus one where indicated.

Supplemental table 1. mAbs used for Flow cytometry

Fluorochrome	Antigen	Clone	Vendor
APC	Anti-Biotin	REA746	Miltenyi
BV785	CD3	UCHT1	BD Biosciences
PE-Cy5	CD3	UHCT1	Beckman Coulter
ECD	CD3	UCHT1	Beckman Coulter
BV421	CD3	SK7	Biolegend
APC	CD3	HIT3a	BD Biosciences
V500	CD14	MφP9	BD Biosciences
BV570	CD14	M5E2	Biolegend
ECD	CD14	RMO52	Beckman Coulter
FITC	CD14	M5E2	BD Biosciences
BUV395	CD16	3G8	BD Biosciences
ECD	CD16	3G8	Beckman Coulter
BV785	CD16	3G8	Biolegend
V500	CD19	HIB19	BD Biosciences
BV570	CD19	HIB19	Biolegend
ECD	CD19	J3-119	Beckman Coulter
BV510	CD19	SJ25C1	BD Biosciences
BV421	CD25	2A3	BD Biosciences
PE-Vio770	CD33	REA775	Miltenyi
BUV395	CD34	581	BD Biosciences
BV711	CD38	HIT2	Biolegend
BV650	CD45	HI30	Biolegend
PerCP-Cy5.5	CD45	H130	BD Biosciences
BV421	CD47	B6H12	BD Biosciences
BUV737	CD56	NCAM16.2	BD Biosciences
ECD	CD56	NHK-1	Beckman Coulter
PE-Cy7	CD56	NCAM16.2	BD Biosciences
Pacific Blue	CD57	HCD57	Biolegend
BV650	CD98	UM7F8	BD Biosciences
BUV395	CD107a	H4A3	BD Biosciences
APC	CD112	TX31	Biolegend
PE-Cy5.5	CD117	104D2D1	Beckman Coulter
PE	CD155	SKII.4	Biolegend
PE	EPCAM	9C4 (#271)	Biolegend
FITC	FcεRIg	polyclonal	Merck-Millipore
BV785	HLA-DR	L243	Biolegend
APC	HLA-E	3D12	Biolegend

PE	HLA-E	3D12	Biolegend
PE-Cy7	HLA-E	3D12	Biolegend
AF700	IFN-γ	B27	BD Biosciences
BV785	IFN-γ	4S.B3	Biolegend
APC	KIR2DL1	REA284	Miltenyi
PE-Cy7	KIR2DL1/S1	EB6B	Beckman Coulter
Biotin	KIR2DL3	REA147	Miltenyi
PE-Cy5.5	KIR2DL3/L2/S2	GL183	Beckman Coulter
AF700	KIR3DL1	DX9	Biolegend
APC-Fire750	KIR3DL1	DX9	Biolegend
Vio-Bright-FITC	NKG2A	REA110	Miltenyi
PE	NKG2C	FAB138P	R&D Systems
APC	NKG2C	REA205	Miltenyi
PE	NKG2C	REA205	Miltenyi
BV711	Streptavidin		BD Biosciences
PE	TIGIT	MBSA43	eBiosciences – Thermo Fisher Scientific
BV650	TNF	MAb11	Biolegend
Aqua	LIVE/DEAD Fixable Aqua Dead Cell Stain Kit		Thermo Fisher Scientific
Near-IR	LIVE/DEAD Fixable Near-IR Dead Cell Stain Kit		Thermo Fisher Scientific
eFluor780	eBiosciences Fixable Viability Dye		Thermo Fisher Scientific
	CellTrace™ Violet Cell Proliferation Kit		Thermo Fisher Scientific
FITC	Cleaved Caspase-3 Staining Kit (FITC)		Abcam
	Recombinant Human KIR2DL1/CD158a Fc Chimera Protein	#1844-KR-050	R&D Systems
	Recombinant Human KIR2DL3/CD158b2 Fc Chimera Protein	#2014-KR-050	R&D Systems
	Recombinant Human NKG2D Fc Chimera Protein		R&D Systems
PE	Goat anti-Human IgG Fc Secondary Antibody	polyclonal	Thermo Fisher Scientific

Supplemental table 2. mAbs used for Mass cytometry

Mass	Antigen	Clone	Vendor
89Y	CD45	HI30	Fluidigm
141Pr	CX3CR1	REA385	Miltenyi
142Nd	CD57	HCD57	Fluidigm
143Nd	CD2	TS1/8	Biolegend
144Nd	CD38	REA572	Miltenyi
145Nd	CXCR3	REA232	Miltenyi
146Nd	CCR2	REA538	Miltenyi
147Sm	CD96	NK92.39	Biolegend
148Nd	CD3	OKT3	Biolegend
148Nd	CD14	RMO52	Fluidigm
148Nd	CD19	HIB19	Biolegend
149Sm	FasL	NOK-1	Biolegend
150Nd	LAG3	11C3C65	Fluidigm
151Eu	CXCR4	REA649	Miltenyi
152Sm	Siglec-7	194211	Fluidigm
153Eu	TIM-3	F38-2E2	Fluidigm
154Sm	NKG2C	REA205	Miltenyi
155Gd	CXCR1	REA958	Miltenyi
156Gd	KIR2DL1/S1	11PB6	Miltenyi
158Gd	KIR2DL1	REA284	Miltenyi
159Tb	GITR	108-17	Biolegend
160Gd	GPR56	CG4	Biolegend
161Dy	PLZF	17.10,.17	Biolegend
162Dy	CD69	FN50	Fluidigm
163Dy	KIR2DL2/S2/L3	GL183	Beckman Coulter
164Dy	TIGIT	MBSA43	Thermo Fisher Scientific
165Ho	CCR5	REA245	Miltenyi
166Er	NKG2D	ON72	Fluidigm
167Er	CCR7	REA108	Miltenyi
168Er	NKp30	P30-15	Miltenyi
169Tm	NKG2A	Z199	Fluidigm
170Er	CXCR2	REA208	Miltenyi
171Yb	DNAM-1	DX11	Fluidigm
172Yb	KIR3DL1	DX9	R&D
173Yb	Granzyme B	GB11	Fluidigm
174Yb	PD-1	EH12.2H7	Fluidigm
175Lu	Perforin	B-D48	Fluidigm
176Yb	CD56	NCAM16.2	Fluidigm
209Bi	CD16	3G8	Fluidigm

Supplemental table 3. GO terms for upregulated genes in Steiner Forest PPI network

Pathway	Total	Expected	Hits	FDR
Cell activation	960	12.6	50	9.35e-15
Leukocyte activation	707	9.3	39	3.9e-12
Lymphocyte activation	601	7.91	36	3.9e-12
Regulation of immune response	727	9.57	39	7.11e-12
Immune response	1430	18.8	55	1.48e-11
Leukocyte differentiation	404	5.32	28	7.03e-11
Regulation of immune system process	1190	15.7	48	1.37e-10
Positive regulation of lymphocyte activation	250	3.29	22	1.83e-10
Hemopoiesis	640	8.42	34	2.15e-10
T cell activation	432	5.68	28	2.15e-10
Lymphocyte differentiation	260	3.42	22	2.92e-10
B cell activation	194	2.55	19	6.62e-10
Hematopoietic or lymphoid organ development	679	8.93	34	8.41e-10
Immune system development	722	9.5	35	9.24e-10
Immune system process	2720	35.8	75	1.09e-09
Cytokine-mediated signaling pathway	374	4.92	25	1.15e-09
Positive regulation of immune system process	739	9.72	34	6.35e-09
Positive regulation of T cell activation	202	2.66	18	7.67e-09
Regulation of lymphocyte activation	360	4.74	23	1.59e-08
B cell differentiation	82	1.08	12	2.88e-08
Regulation of T cell activation	279	3.67	20	2.98e-08
T cell differentiation	186	2.45	16	1.14e-07
Regulation of response to stimulus	3360	44.2	80	1.78e-07
Positive regulation of response to stimulus	1550	20.4	48	3.52e-07
Response to stress	4150	54.6	91	4.62e-07
Positive regulation of immune response	487	6.41	24	8.01e-07
Response to wounding	1310	17.3	42	1.29e-06
Regulation of body fluid levels	680	8.95	28	2.19e-06
Blood coagulation	564	7.42	24	1.1e-05
Coagulation	568	7.47	24	1.21e-05
Hemostasis	570	7.5	24	1.24e-05
Response to radiation	345	4.54	18	1.79e-05
Defense response	1510	19.9	43	1.79e-05
Interaction with host	426	5.61	20	2.08e-05
Regulation of immune effector process	249	3.28	15	2.44e-05
Production of molecular mediator of immune response	130	1.71	11	2.53e-05
Regulation of apoptotic process	1540	20.2	43	2.53e-05
Activation of immune response	399	5.25	19	2.88e-05
Regulation of programmed cell death	1550	20.4	43	3.27e-05
Wound healing	700	9.21	26	3.33e-05
Immune effector process	576	7.58	23	4.12e-05
Response to organic substance	2500	32.9	59	4.18e-05
Innate immune response	638	8.39	24	6.52e-05
Regulation of cell differentiation	1290	17	37	7.99e-05
Positive regulation of cell proliferation	786	10.3	27	7.99e-05
Cell migration	1050	13.9	32	0.000125
Positive regulation of developmental process	817	10.8	27	0.000156
Peptidyl tyrosine phosphorylation	228	3	13	0.000173
Positive regulation of metabolic process	2690	35.4	60	0.000183
Peptidyl tyrosine modification	230	3.03	13	0.000183
Viral reproductive process	597	7.86	22	0.000201
Regulation of cellular component organization	1520	20.1	40	0.000226
Response to ionizing radiation	112	1.47	9	0.000256
Regulation of developmental process	1880	24.7	46	0.000256
Regulation of protein metabolic process	1820	24	45	0.000268
Adaptive immune response	241	3.17	13	0.000268
Inflammatory response	569	7.49	21	0.00028
Regulation of myeloid cell differentiation	145	1.91	10	0.000307
Cell proliferation	1900	25	46	0.000329
Positive regulation of biological process	5500	72.3	100	0.000361
Positive regulation of cellular metabolic process	2530	33.2	56	0.000389
Negative regulation of apoptotic process	679	8.93	23	0.000389
Response to abiotic stimulus	876	11.5	27	0.000395
Adaptive immune response based on somatic recombination of immune receptors built from immunoglobulin superfamily domains	218	2.87	12	4,00E-04
Regulation of protein modification process	1250	16.4	34	0.000422
Negative regulation of programmed cell death	691	9.09	23	0.000481
Negative regulation of signal transduction	790	10.4	25	0.000491

Positive regulation of cell migration	263	3.46	13	0.000542
Cell surface receptor signaling pathway	3340	43.9	68	0.000542
Positive regulation of cellular process	4780	62.9	89	0.000571
Response to light stimulus	229	3.01	12	0.000584
Homeostasis of number of cells	196	2.58	11	0.000641
Exocytosis	309	4.07	14	0.000656
Leukocyte migration	309	4.07	14	0.000656
Interphase of mitotic cell cycle	435	5.72	17	0.000674
Positive regulation of cell differentiation	571	7.51	20	0.000688
Regulation of multicellular organismal process	2480	32.6	54	0.000748
Epidermal growth factor receptor signaling pathway	167	2.2	10	0.000752
Intrinsic apoptotic signaling pathway	135	1.78	9	0.000752
Interphase	443	5.83	17	0.000783
Positive regulation of protein metabolic process	1080	14.3	30	0.000783
Apoptotic process	2130	28	48	0.000877
Positive regulation of transcription, DNA-dependent	1260	16.6	33	0.000901
Regulation of cell proliferation	1430	18.8	36	0.000917
Peptidyl amino acid modification	739	9.72	23	0.00101
Response to UV	112	1.47	8	0.00106
Regulation of cellular protein metabolic process	1560	20.5	38	0.0011
Programmed cell death	2160	28.4	48	0.00111
Negative regulation of transcription from RNA polymerase II promoter	552	7.26	19	0.00111
Positive regulation of RNA metabolic process	1330	17.5	34	0.00111
T cell proliferation	147	1.93	9	0.00123
Myeloid cell differentiation	296	3.89	13	0.0013
Negative regulation of metabolic process	1820	24	42	0.00148
Regulation of transferase activity	768	10.1	23	0.00161
Nucleocytoplasmic transport	388	5.11	15	0.00161
Nuclear transport	392	5.16	15	0.00178
Positive regulation of cytokine biosynthetic process	66	0.868	6	0.00184
Positive regulation of nucleobase-containing compound metabolic process	1490	19.6	36	0.00184
Regulation of mitotic cell cycle	351	4.62	14	0.00184
Regulation of cell cycle	886	11.7	25	0.00198
Regulation of kinase activity	743	9.78	22	0.00246
Regulation of phosphorylation	1070	14	28	0.00266
Regulation of protein kinase activity	698	9.18	21	0.00269
Viral reproduction	803	10.6	23	0.00278
Interleukin_2 production	47	0.618	5	0.00278
Negative regulation of cellular component organization	370	4.87	14	0.00292
Negative regulation of response to stimulus	967	12.7	26	0.00292
Protein complex assembly	861	11.3	24	0.00295
Regulation of peptidyl tyrosine phosphorylation	171	2.25	9	0.00319
Regulation of cytokine production	513	6.75	17	0.00321
Positive regulation of T cell proliferation	75	0.987	6	0.00326
Negative regulation of cellular metabolic process	1660	21.9	38	0.00326
Regulation of cell-cell adhesion	77	1.01	6	0.00368
Regulation of protein phosphorylation	987	13	26	0.00368
Negative regulation of transcription, DNA-dependent	987	13	26	0.00368
Cellular response to stress	1620	21.4	37	0.00398

Supplemental table 4. GO terms for downregulated genes in Steiner Forest PPI network

Pathway	Total	Expected	Hits	FDR
Negative regulation of metabolic process	1820	19.9	55	2.37e-10
Negative regulation of cellular metabolic process	1660	18.2	52	2.37e-10
Negative regulation of signal transduction	790	8.63	34	9.87e-10
Negative regulation of cellular process	4110	44.8	85	2.4e-09
Regulation of signal transduction	2440	26.6	61	6.57e-09
Negative regulation of response to stimulus	967	10.6	36	6.57e-09
Regulation of I-kappaB kinase/NF-kappaB cascade	210	2.29	17	1.55e-08
Cytokine_mediated signaling pathway	374	4.08	21	7.53e-08
Negative regulation of biological process	4590	50.1	87	7.53e-08
I-kappaB kinase/NF-kappaB cascade	246	2.69	17	1.26e-07
Regulation of apoptotic process	1540	16.8	43	2.67e-07
Regulation of programmed cell death	1550	17	43	2.75e-07
Negative regulation of transcription, DNA-dependent	987	10.8	33	2.75e-07
Apoptotic process	2130	23.2	52	2.75e-07
Innate immune response	638	6.97	26	2.75e-07
Negative regulation of cellular biosynthetic process	1220	13.3	37	3.58e-07
Programmed cell death	2160	23.5	52	3.79e-07
Negative regulation of biosynthetic process	1240	13.6	37	4.96e-07
Negative regulation of nucleobase-containing compound metabolic process	1130	12.3	35	4.96e-07
Negative regulation of RNA metabolic process	1020	11.2	33	5.1e-07
Response to organic substance	2500	27.3	56	9.15e-07
Protein import into nucleus	228	2.49	15	9.82e-07
Nuclear import	232	2.53	15	1.19e-06
Interaction with host	426	4.65	19	6.26e-06
Regulation of defense response	519	5.67	21	6.69e-06
Nucleocytoplasmic transport	388	4.24	18	6.99e-06
Intracellular receptor mediated signaling pathway	270	2.95	15	7.47e-06
Nuclear transport	392	4.28	18	7.59e-06
Protein import	272	2.97	15	7.68e-06
Regulation of response to stimulus	3360	36.7	65	8.69e-06
Regulation of nucleocytoplasmic transport	172	1.88	12	9.82e-06
Regulation of intracellular transport	290	3.17	15	1.59e-05
Regulation of molecular function	2250	24.5	49	1.61e-05
Regulation of cytokine production	513	5.6	20	1.79e-05
Myeloid cell differentiation	296	3.23	15	1.89e-05
Organ development	3290	35.9	63	1.93e-05
Regulation of developmental process	1880	20.5	43	2.5e-05
Central nervous system development	784	8.56	25	2.56e-05
Cell surface receptor signaling pathway	3340	36.4	63	2.92e-05
Response to chemical stimulus	3830	41.8	69	3.69e-05
Negative regulation of transcription from RNA polymerase II promoter	552	6.03	20	4.65e-05
Regulation of transforming growth factor beta receptor signaling pathway	107	1.17	9	4.7e-05
Regulation of cell proliferation	1430	15.6	35	6.37e-05
Defense response	1510	16.5	36	8.1e-05
Intracellular protein kinase cascade	1140	12.4	30	8.22e-05
Negative regulation of cell proliferation	585	6.39	20	9.97e-05
Negative regulation of transferase activity	189	2.06	11	0.000119
Regulation of transcription from RNA polymerase II promoter	1610	17.6	37	0.000122
Protein targeting	545	5.95	19	0.000123
Regulation of cell differentiation	1290	14.1	32	0.000123
Positive regulation of developmental process	817	8.92	24	0.000132
Response to stress	4150	45.3	71	0.000132
Positive regulation of defense response	273	2.98	13	0.000136
Regulation of protein metabolic process	1820	19.9	40	0.000136
Positive regulation of signal transduction	998	10.9	27	0.000142
Regulation of multicellular organismal process	2480	27.1	49	0.000167
Regulation of immune system process	1190	13	30	0.000172
Positive regulation of transcription, DNA-dependent	1260	13.7	31	0.000173
Regulation of sequence-specific DNA binding transcription factor activity	372	4.06	15	0.000184
G1 phase	49	0.535	6	0.00019
Negative regulation of apoptotic process	679	7.41	21	0.000195
Negative regulation of phosphorylation	246	2.69	12	2,00E-04
Regulation of catalytic activity	1730	18.9	38	2,00E-04
Cytokine production	576	6.29	19	0.000203
Positive regulation of transcription from RNA polymerase II promoter	800	8.73	23	0.000223
Regulation of protein import into nucleus	137	1.5	9	0.000223
Negative regulation of phosphate metabolic process	293	3.2	13	0.000228
Negative regulation of programmed cell death	691	7.54	21	0.000229

Negative regulation of binding	78	0.852	7	0.000251
Immune response	1430	15.6	33	0.000262
Defense response to virus	215	2.35	11	0.000262
Cell proliferation	1900	20.8	40	0.000271
Multi-organism process	1710	18.6	37	0.000304
Regulation of myeloid cell differentiation	145	1.58	9	0.000315
Regulation of cell cycle	886	9.67	24	0.000336
Positive regulation of catalytic activity	1070	11.7	27	0.000345
Regulation of gene expression	4480	48.9	73	0.000373
Positive regulation of cytokine production	268	2.93	12	0.000379
Immune system development	722	7.88	21	0.000379
Positive regulation of RNA metabolic process	1330	14.6	31	0.000389
Intracellular signal transduction	2450	26.7	47	4,00E-04
Regulation of immune response	727	7.94	21	0.000404
Regulation of transcription, DNA-dependent	3770	41.2	64	0.000427
Regulation of nucleobase-containing compound metabolic process	4540	49.5	73	0.000519
Immune effector process	576	6.29	18	0.000519
Positive regulation of sequence-specific DNA binding transcription factor activity	198	2.16	10	0.000563
Immune system process	2720	29.7	50	0.000578
Cell cycle	1860	20.3	38	0.000694
Interphase of mitotic cell cycle	435	4.75	15	0.000723
Negative regulation of protein metabolic process	540	5.9	17	0.000732
Viral reproductive process	597	6.52	18	0.00077
Regulation of transferase activity	768	8.39	21	0.000778
Interphase	443	4.84	15	0.00085
Reproductive process	1740	19	36	0.00086
Positive regulation of metabolic process	2690	29.4	49	0.000867
Embryo development	1080	11.8	26	0.000907
Cell cycle process	1420	15.4	31	0.00097
Positive regulation of response to stimulus	1550	17	33	0.000997
Cellular response to stress	1620	17.7	34	0.00103
Positive regulation of nucleobase-containing compound metabolic process	1490	16.3	32	0.00103
Regulation of cellular protein metabolic process	1560	17	33	0.00103
Regulation of RNA metabolic process	3900	42.6	64	0.00106
Intracellular protein transport	793	8.66	21	0.00109
Transcription initiation from RNA polymerase II promoter	219	2.39	10	0.00109
Cell development	1840	20.1	37	0.00109
Hematopoietic or lymphoid organ development	679	7.41	19	0.00112
G1 phase of mitotic cell cycle	47	0.513	5	0.00112
Reproduction	1860	20.3	37	0.00118
Enzyme linked receptor protein signaling pathway	1180	12.8	27	0.00118
Negative regulation of cellular protein metabolic process	463	5.06	15	0.00118
Positive regulation of cell differentiation	571	6.23	17	0.00118
Multicellular organismal development	5720	62.4	85	0.00118
Cellular protein catabolic process	518	5.66	16	0.0012
Regulation of protein modification process	1250	13.6	28	0.00127

Extended Methods

Flow- and mass cytometry

Details of all antibodies used for flow cytometry are found in sTable1 and for mass cytometry in sTable2. Recombinant Human NKG2D Fc Chimera Protein (#1299-NK-050, R&D Systems) was biotinylated using the One-Step Antibody Biotinylation Kit (Miltenyi Biotec) as per manufacturer's recommendation. For all surface antibodies, cells were stained in PBS containing 2% FBS and 2 mM EDTA (Thermo Fisher, USA) for 15 min at room temperature followed by two washes. A second extracellular stain and incubation was performed with streptavidin and the pan-KIR binding antibodies KIR2DL2/S2/L3 and KIR2DL1/S1. After washing, cells were fixed for 15-20 min at 4 °C using BD Cytofix/Cytoperm™ Fixation and Permeabilization Solution (BD Biosciences). After two washes with BD Perm/Wash™ Buffer (BD Biosciences), intracellular markers were stained in this buffer for 30 min at room temperature. For HLA-C1/C2 expression, cells were stained with recombinant human KIR2DL1/CD158a or KIR2DL3/CD158b2-Fc Chimera Proteins (R&D systems) at 30 µg/ml in PBS 60 mins on ice, washed twice and incubated 15 mins at room temperature with Goat anti-Human IgG Fc Secondary Antibody, conjugated to PE. Samples were incubated with the secondary antibody only or isotype IgG1-PE as controls. Cells were fixed and acquired as described above. Flow cytometry samples were acquired on a BD LSRII or LSR Fortessa flow cytometer (BD Biosciences). Acquired data were analyzed in FlowJo v.10.6 (BD Biosciences) gated on live $CD19^{-}CD3^{-}CD56^{+}$ single cells or $CTV^{+}CD56^{-}$ target cells for cytotoxicity assays. AML blasts were defined by low CD45 expression. For visualization of flow cytometry data, t-Distributed Stochastic Neighbor Embedding (t-SNE), an unsupervised nonlinear dimensionality reduction algorithm, was employed in FlowJo software with default settings and included all fluorescent markers stained for. For mass cytometry experiments, cells were stained with Cell-ID Intercalator-103Rh (Fluidigm) for viability assessment followed by an Fc

blocking reagent and a surface antibody cocktail. Antibodies that were not available pre-labelled were conjugated to metal isotopes using Maxpar X8 Antibody Labeling Kits (Fluidigm). Cells were fixed with 2% formaldehyde in Maxpar PBS (Fluidigm). Samples were washed, permeabilized and barcoded using the Cell-ID 20-Plex Pd Barcoding Kit (Fluidigm) before being pooled. Samples were then resuspended in cold methanol and stored overnight at -20 °C. Upon acquisition, cells were stained with an intracellular antibody cocktail, labeled with Cell-ID Intercalator-Ir (Fluidigm) and resuspended in Maxpar Cell Acquisition Solution (Fluidigm). EQ Four Element Calibration Beads (Fluidigm) were added to the cells before analysis on a Helios CyTOF instrument (Fluidigm). FCS files were concatenated, normalized and debarcoded using Helios software (Fluidigm), and gated using FlowJo v.10 (BD Biosciences). For subsequent analysis, data was imported into R (R Core Team, 2019) using the flowCore package, and transformed using arcsinh(x/5). For mass-cytometry data, t-SNE was performed using the Rtsne R package with default settings and results were visualized using the ggplot2 R package.

Cellular indexing of transcriptomes and epitopes by sequencing - CITE-Seq.

CITE-seq was performed as outlined in Biolegend 'TotalSeqTM-A Antibodies and Cell Hashing with 10x Single Cell 3' Reagent Kit v3 3.1 Protocol' with minor modifications. Briefly, cells were stained with CD56-biotin (REA 196), followed by TotalSeq antibodies and TotalSeq streptavidin-PE and Live/Dead Aqua (Invitrogen) and subsequently sorted for viable $CD56^+$ cells by flow cytometry. Day 0 cells from the same donor were thawed and recovered in IL-15 (3 ng/ml, Miltenyi) overnight prior to staining and sorting. To distinguish day 0 and day 11 cells, streptavidin-PE conjugated to different oligos were used, and equal number of sorted viable $CD56^+$ cells from the two cell preparations were pooled as one sample. This was followed by standard 10X Genomics library preparation and sequencing workflow (Genomics

Core Facility UiO, Oslo, Norway). Sequencing was performed with the recommended read lengths on the NextSeq500 sequencer (Illumina). Data were demultiplexed using bcl2fastq2 (Illumina) and further processed with the Cell Ranger version 6.0.1 software package to generate raw count-matrix files. The antibody-derived tags (ADTs) were counted using the package CITE-Seq-Count[2]. CITE-Seq data was analyzed using Scanpy[3] as follows: During pre-processing cells were filtered out based on number of genes and reads in each cell (minimum 300 genes, maximum 30 000 total counts) and genes were filtered based on number of cells in which the genes were expressed (minimum 3 cells). Cells with more than 10% mitochondrial reads were also filtered out. Cells with expression of CD3 were filtered out together with cells expressing both day 0 and day 11 ADTs. The remaining cells (n=8013) were analyzed using the probabilistic model totalVI[4]. This model was used to get a representation of the cells that were used for clustering and for embedding using UMAP, get denoised expression values for both the ADTs and mRNA, and to perform the statistical tests to identify differentially expressed (DE) genes. Heatmaps, UMAP plots, violin plots and dot plots were generated using Scanpy[3]. The p-values and fold change computed from the DE framework in totalVI were plotted as volcano plots using bioinfokit[5]. The genes down- and upregulated in CAR T cells after continuous antigen exposure were extracted from Good et al.[1] and for both gene sets the overlap with the genes upregulated in the day 11 CITE-Seq cluster was shown in Venn diagrams. AUCell[6] was used to identify the activity of a T cell-derived exhaustion signature from Feucht et al.[7] in the CITE-Seq data and the AUC scores were plotted as violin plots showing the activity of this signature in the various clusters.

Tumor cell lines

The K562 cell line (chronic myeloid leukemia) and 721.221 (EBV-transformed B cell line) were obtained from ATCC. HL-60 (acute myeloid leukemia) was obtained from the Miller lab.

PANC-1 (Pancreatic ductal adenocarcinoma) and A549 (lung adenocarcinoma) were obtained from Fate Therapeutics. K562, A549 and PANC-1 along with NALM-6 (B cell acute lymphoblastic leukemia) and BJAB (Burkitt's Lymphoma) were re-authenticated using STR fingerprinting (ATCC). The K562, 721.221, BJAB and NALM-6 cell lines were cultured in RPMI-1640 (Thermo Fisher) with 10% FBS and 1 mM L-glutamine (Thermo Fisher) ('complete RPMI') and with or without 100 mg/ml of penicillin/streptomycin (Invitrogen). HL-60 was grown in IMDM, A549 and PANC-1 in DMEM, all with 10% FBS and with or without 100 mg/ml of penicillin/streptomycin (Invitrogen). Cell lines were KIR-ligand genotyped with PCR-based KIR-HLA Ligand kit (Olerup SSP). All cell lines were mycoplasma-tested using one of the following reagents: MycoAlert™ PLUS Mycoplasma Detection Kit (Lonza), the PCR-based LookOut Mycoplasma (Sigma Aldrich), or Mycoplasma check (Eurofins Genomics).

Flow cytometry-based NK cell functional assays

NK cell degranulation and cytokine production was evaluated by mixing ADAPT-NK products at different E:T ratios with tumor targets and incubating in complete RPMI in 96-well U-bottom plates for 6 h at 37 °C and 5% CO_2. Monensin (GolgiStop, 1:1500, BD Biosciences), Brefeldin A (GolgiPlug, 1:1000, BD Biosciences) and anti-CD107a were added 1 h into the 6 h co-culture. To measure ADCC, MabThera (1 µg/ml) was added to co-culture experiments with 721.221 cells. Phorbol-12-myristate-13-acetate (PMA) (50 ng/ml) + ionomycin (1 µg/ml) (Sigma) was used as positive control. NK cell cytotoxicity was evaluated by mixing ADAPT-NK products at different E:T ratios with single target cell lines pre-stained with 2 µM of CellTrace Violet (Thermo Fisher) and incubating in 96-well V-bottomed plates for 6 h at 37 °C and 5% CO_2. FITC-DEVD-FMK (Abcam), a caspase-3 inhibitor used to detect the active/cleaved form of Caspase-3 was added at the start of the incubation and cells were

subsequently stained with eFluor780 Fixable viability dye (Thermo Fisher). All samples were fixed and acquired on a flow cytometer as described above. Dead cells were defined as CellTrace^{+} Caspase-3^{+} and/or dead cell marker (DCM)$^{+}$ and specific cytotoxicity calculated as: ($\%\ dead^{\ experimental}$ - $\%\ dead^{\ target\ only}$) ÷ (100% - $\%\ dead^{\ target\ only}$) x 100%. For competitive cytotoxicity assays, HLA-C1- and HLA-C2-dimer expressing K562 were stained with either high (2 μM) or low (0.5 μM) concentrations of CellTrace Violet respectively, prior to being mixed at a 1:1 ratio and subsequently seeded at multiple E:T ratios with ADAPT-NK cells. The two different target cells were then identified based on CellTrace^{+} high or low, and in these populations the frequency of live (Caspase-3^{-} and/or DCM^{-}) remaining in the culture out of the total live CTV^{+} cells was determined. Cytokine stimulations with IL-12 (10 ng/ml) and IL-18 (10 ng/ml) (both Biotechne) were performed for 25 h at 37 °C and 5% CO_2, and Monensin and Brefeldin A were added after 20 h.

Genetic cell engineering

In brief, K562 cells (ATCC Cat: CCL-243) were engineered by Fate Therapeutics using an in-house third-generation lentiviral transfer plasmid designed to contain a chimeric protein with the HLA-G leader peptide (1-24) and the mature HLA-E*0103 (22-358) driven by an EF1α promoter. Lentivirus was produced in Lenti-X™ 293T cells (Clontech 632180) using the second-generation packaging system that includes a transfer plasmid, a packaging plasmid, for expression of gag, pol, tat and rev, and an envelope plasmid, for expression of envelope protein VSV-G. The transduced population was sorted to enrich for cells expressing high levels of HLA-E. For HLA-C and -E variants, K562 were engineered in-house using VSV-G-pseudotyped lentiviral particles with a mammalian LeGO-G2 expression vector, to express the following synthetic proteins: β2m–HLA-C1 single chain dimer (HLA-C1-dimer): *B2M* signal peptide sequence and mature *B2M* (without STOP-codon) fused covalently to mature *HLA*-

*C*07:01* (without STOP-codon) through a flexible $(G_4S)_4$ linker sequence, followed by a T2A peptide sequence and murine *Thy1.1* (*CD90.1*) ; β2m–HLA-C2 singe chain dimer (HLA-C2-dimer): *B2M* signal peptide sequence and mature *B2M* (without STOP-codon) fused covalently to mature *HLA-C*04:01* (without STOP-codon) through a flexible a $(G_4S)_4$ linker sequence, followed by a T2A peptide sequence and murine *Thy1.2* (*CD90.2*); HLA-G_{3-11}–β2m–HLA-E single chain trimer (HLA-E-trimer): *B2M* signal peptide sequence and the *HLA-G*$_{3-11}$ signal peptide sequence (VMAPRTLFL) fused covalently by a flexible $(G_4S)_3$ linker sequence to mature *B2M* (without STOP-codon), which is further covalently linked to mature *HLA-E*01:01* by a flexible $(G_4S)_4$ linker sequence. Expression cassettes were sub-cloned into the mammalian expression vector LeGO-G2 (kind gift from Boris Fehse, Addgene plasmid #251917; http://n2t.net/addgene:25917; RRID: Addgene_25917) after removing EGFP. LeGO-HLA-C1-dimer, LeGO-HLA-C2-dimer, and LeGO-HLA-E-trimer were used to generate VSV-G-pseudotyped lentiviral particles. For production of VSV-G-pseudotyped lentiviral particles, 22 x 10^6 LentiX 293T cells (Takara) were plated into T125 flask one day prior to transfection with 15 µg of LeGO expression vector, 10 µg pRSV-Rev (Addgene plasmid #12253), 15 µg pMDLg/pRRE (Addgene plasmid #12251) and 5 µg pCMV-VSV-G (Addgene plasmid #8454) using Lipofectamine 3000 (Invitrogen). Supernatant containing lentiviral particles was harvested at 24 and 48 h post transfection and concentrated using LentiX concentrator (Takara). Viral titers were determined using Lenti-X GoStix (Takara). Concentrated virus was stored as aliquots at -80 ℃ until use. Wildtype K562 cells were then transduced with 20 MOI of lentiviral particles at 2,5 x10^5 / 24-well in a total volume of 1 ml. The plates were centrifuged at 900 *g* for 1 h at 32 ℃ followed by incubation at 37 ℃ overnight. Media was exchanged the next day and cells were cultivated for >5 passages. After >5 passages, genetically engineered K562 lines were sorted on a MA900 cell sorter (Sony) for high HLA-C-dimer expression using recombinant human KIR2DL3 Fc chimera proteins and

KIR2DL3 Fc chimera proteins, respectively or sorted for high HLA-E-trimer expression using an anti-HLA-E antibody (3D12, BioLegend). Sorted cells were routinely monitored for HLA-C-dimer and HLA-E-trimer expression and tested for presence of mycoplasma (Eurofins Mycoplasma check). Further, NALM-6 were engineered to knock-out HLA-E using Cas9 and a pool of synthetic guide RNAs (sgRNA) (5'- AUUUCCACACUUCCGUGUCC-3', 5'-ACAACGACGCCGCGAGUCCG-3' and 5'-GGGGUCAGAGUAUUGGGACC-3') (CRISPRevolution sgRNA EZ Kit, Synthego). 180 pmol sgRNA and 20 pmol Cas9 (Synthego) were used to form ribonucleoprotein (RNP) complexes. 1.5 x 10^5 cells in 3P buffer (5 mM KCl, 15 mM MgCl2, 90 mM NaCl, 10 mM Glucose, 0.4 mM Ca(NO3)2, 40 mM Na2HPO4/NaH2PO4 pH7.2) were mixed with RNP and electroporated using Lonza 4D-Nucleofector system with pulse code CV-104. Cells were grown for 7 days before single cells were sorted on a FACS Aria II (BD Biosciences) to establish multiple clones in 96-well round bottom plates. DNA sequencing and flow cytometry confirmed HLA-E depletion in the selected clones used in the study. HLA-E sgRNAs further targeted the HLA-C locus resulting in a combined KO for this line.

Serial killing assays

The cytotoxic potential of individual NK cells was evaluated using a previously described microwell chip screening assay[8]. Briefly, NK cells labelled with 5 µg/ml CellTrace Yellow and target cells labelled with 5 µg/ml CellTrace Far Red (Thermo Fisher) were seeded in a microwell chip containing complete RPMI supplemented with 100 ng/ml Sytox Green (Thermo Fisher). Cells stochastically distributed in the 8064 60-µm-wide wells at an average effector to target ratio of 1:5. HLA-C matched and -mismatched co-cultures with the same ADAPT-NK product were investigated simultaneously in different compartments of the chip. The co-cultures were imaged every 3 h for 15 h using an inverted confocal microscope, LSM 880 (Carl

Zeiss AG) equipped with a 10x/0.5 Plan-Achromat objective and an environmental control unit (37ºC, CO_2 5%). The images were processed using a custom-built MATLAB script whereby live and dead cells were quantified at all time points. For each condition, a minimum of 500 wells containing a single NK cell at start along with at least 4 live target cells were included for analysis. Target cell death was adjusted for spontaneous death using wells containing only target cells.

IncuCyte measurement of tumor killing

Tumor killing was measured in real time using the IncuCyte® S3 platform. Target cells stably expressing NucLight Red (Essen Biosciences) were selected for NucLight Red expression after thawing with 2 µg/mL puromycin for 72 h, screened by flow cytometry for uniform NucLight Red expression and allowed to rest without puromycin for at least 48 h (1 passage) before assay. Target cells were seeded at 5000 cells/well in 200 uL of complete media and allowed to attach overnight in clear, 96-well flat-bottom plates (Thermo Fisher, cat. #167008). Wells used for target cells which habitually grow in suspension (HL60, K562, Bjab, Nalm6) were pre-coated with Poly-L-Ornithine solution (Sigma/Merck, cat #A-004-M). At assay start half of the media was removed and ADAPT-NK cells were serially diluted and added to the wells in SCGM (CellGenix) with 50 IU/mL IL-2 at different E:T ratios. Images (3/well) from at least two technical replicates for each condition were acquired every 90 min for 48 h, using a 10x objective lens and analyzed by IncuCyte Controller v2020A (Essen Biosciences). Graphed readouts represent percentage live target cells (NucLight Red^+). To obtain percentage of live cells, live target cell count in each well was normalized by division to timepoint 0 h (T0), and then to the number of live cells in the "target cell only" control group, as calculated in the following equation: % Live cells = [(Tn/T0) test / (Tn/T0) ctrl] x 100. The means of the technical replicates for each condition were compiled for n=4-9 donors, tested in at least two

independent experiments for each target cell, and are displayed as mean (± SD). Area Under Curve for each condition was graphed and analyzed.

In vivo AML tumor model

Fifteen male 9-11 weeks old NOD.Cg-PrkdcscidIl2rgtm1Wjl/SzJ mice (NSG, Jackson Laboratories) mice were injected intravenously with HL-60 cells stably expressing firefly luciferase ($1.5x10^6$/mouse). Four control mice on the same background received no injections. After allowing tumors to engraft for 4 days, bioluminescence imaging was performed, and mice were randomized into 3 groups. Mice in the first group received no treatment (tumor alone). Mice in the second group received intravenous injections of HLA-C/KIR matched ADAPT-NK cells (flat-dose 5 $x10^6$/mouse) expanded as above. Mice in the third group received intravenous injections of HLA-C/KIR mismatched ADAPT-NK cells (flat-dose $5x10^6$/mouse). Mice receiving NK cell injections were also injected intraperitoneally with IL-15 (6ug/mouse, National Cancer Institute) twice weekly for three weeks. Bioluminescence imaging was performed weekly to track tumor burden using the IVIS Spectrum (Perkin-Elmer). Images were analyzed using Living Image software (Perkin-Elmer). D-Luciferin Sodium Salt (GoldBio) was dissolved into DPBS at a concentration of 30 mg/ml and injected intraperitoneally at a dose of 3 mg/20 g body weight.

References extended methods

1. Good, C.R. *et al.* An NK-like CAR T cell transition in CAR T cell dysfunction. *Cell* **184**, 6081-6100 e6026 (2021).

2. Gui, P.R.b.B.F.s.G. Hoohm/CITE-seq-Count: 1.4.2. Zenodo; 2019.

3. Wolf, F.A., Angerer, P. & Theis, F.J. SCANPY: large-scale single-cell gene expression data analysis. *Genome Biol* **19**, 15 (2018).

4. Gayoso, A. *et al.* Joint probabilistic modeling of single-cell multi-omic data with totalVI. *Nat Methods* **18**, 272-282 (2021).

5. Bedre, R. reneshbedre/bioinfokit: Bioinformatics data analysis and visualization toolkit. . Zenodo; 2021.

6. Aibar, S. *et al.* SCENIC: single-cell regulatory network inference and clustering. *Nat Methods* **14**, 1083-1086 (2017).

7. Feucht, J. *et al.* Calibration of CAR activation potential directs alternative T cell fates and therapeutic potency. *Nat Med* **25**, 82-88 (2019).

8. Guldevall, K. *et al.* Microchip Screening Platform for Single Cell Assessment of NK Cell Cytotoxicity. *Front Immunol* **7**, 119 (2016).

Adaptive single-KIR⁺NKG2C⁺ NK cells expanded from select superdonors show potent missing-self reactivity and efficiently control HLA-mismatched acute myeloid leukemia

Authors:
A. Haroun-Izquierdo, M. Vincenti, H. Netskar, H. van Ooijen, B. Zhang, L. Bendzick, M. Kanaya, P. Momayyezi, S. Li, M. Thune Wiiger, H. J. Hoel, S. Zandstra Krokeide, V. Kremer, G. Tjønnfjord, S. Berggren, K. Wikström, P. Blomberg, E. Alici, M. Felices, B. Onfelt, P. Hoglund, B. Valamehr, H.G. Ljunggren, A. Bjorklund, Q. Hammer, L. Kveberg, F. Cichocki, J. S. Miller, K.-J. Malmberg* and E. Sohlberg*

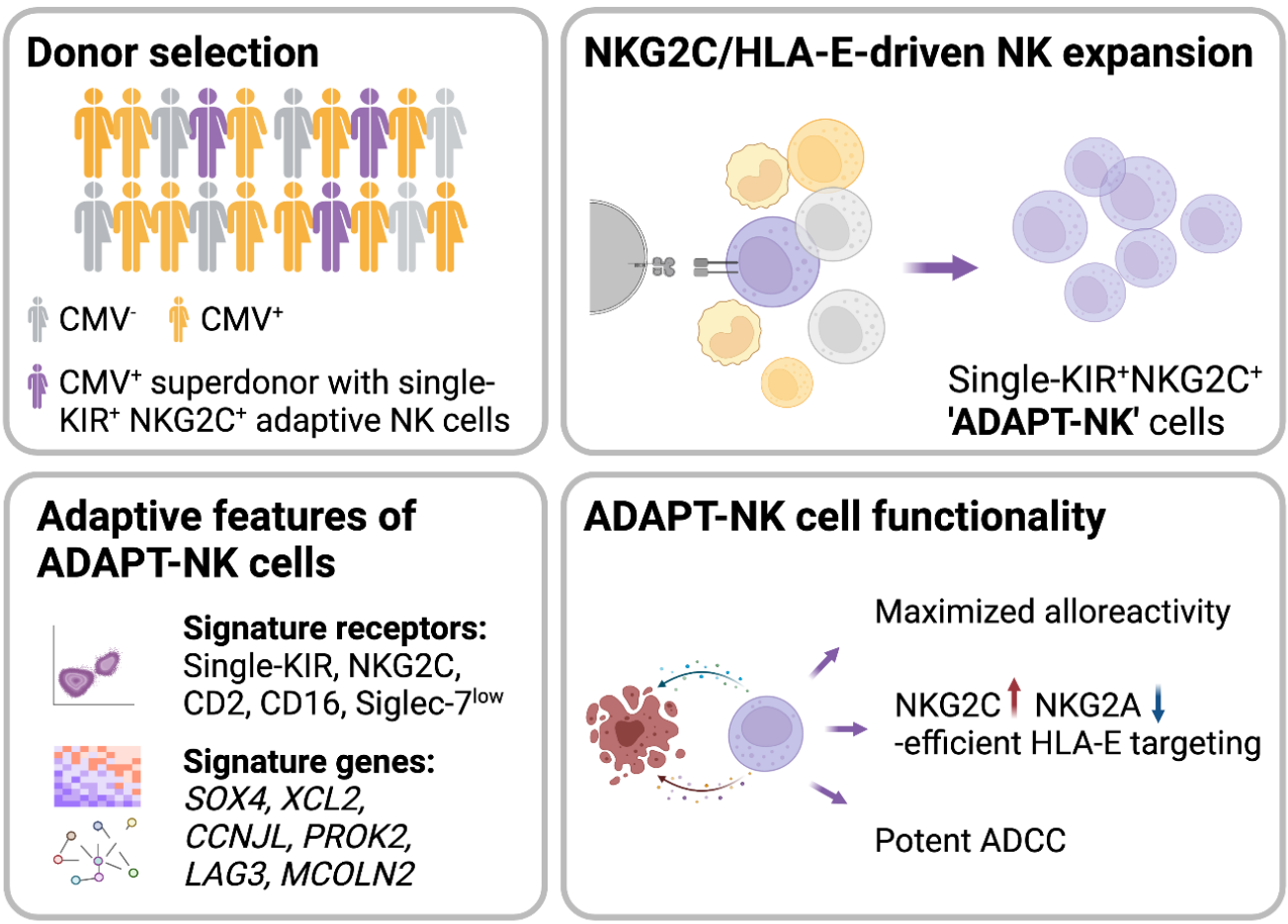

In brief:

1. Novel GMP-compliant protocol to expand single self-KIR⁺ adaptive NK cells from third-party 'superdonors'.
2. Strong alloreactivity in a mouse model of AML as well as against primary AML blasts.
3. ADAPT-NK cells overcome the HLA-E checkpoint and display potent ADCC